Temperature and magnetic-field dependence of quantum creep in various high-T_c superconductors

A. F. Th. Hoekstra
Institute COMPAS and Faculty of Physics and Astronomy, Vrije Universiteit, De Boelelaan 1081, 1081 HV Amsterdam, The Netherlands

A. M. Testa
Institute COMPAS and Faculty of Physics and Astronomy, Vrije Universiteit, De Boelelaan 1081, 1081 HV Amsterdam, The Netherlands and ICMAT CNRS, Area della Ricerca, Rome, Italy

G. Doornbos
Institute COMPAS and Faculty of Physics and Astronomy, Vrije Universiteit, De Boelelaan 1081, 1081 HV Amsterdam, The Netherlands

J. C. Martinez
Institute COMPAS and Faculty of Physics and Astronomy, Vrije Universiteit, De Boelelaan 1081, 1081 HV Amsterdam, The Netherlands and Institut für Physik, Johannes Gutenberg-Universität, Staudingerweg 7, D-55099 Mainz, Germany

B. Dam and R. Griessen
Institute COMPAS and Faculty of Physics and Astronomy, Vrije Universiteit, De Boelelaan 1081, 1081 HV Amsterdam, The Netherlands

B. I. Ivlev
Instituto de Fisica, Universidad Autonoma de San Luis Potosi, Alvaro Obregon 64, 78000 San Luis Potosi, Mexico

M. Brinkmann and K. Westerholt
Institut für Experimentalphysik/Festkörperphysik, Ruhr-Universität Bochum, D-44780 Bochum, Germany

W. K. Kwok and G. W. Crabtree
Materials Science Division, Argonne National Laboratory, 9700 South Cass Avenue, Argonne, Illinois 60439
(Received 13 August 1998)

To investigate the quantum tunneling of almost macroscopic vortex segments we measured the normalized relaxation rate Q of superconducting currents for various high-T_c superconductors (HTS's) down to 100 mK in magnetic fields up to 7 T. At fields below $\cong 0.5$ T, Q is essentially independent of T in the temperature regime between thermally activated and quantum motion as theoretically expected. However, at higher fields, we find an unexpected linear T dependence of Q persisting down to the lowest temperatures in all investigated samples. Since these compounds were chosen to represent the distinct classes of dirty and clean HTS's, the extrapolated $Q(T=0)$ values are used to discuss the theoretical models for quantum creep in the clean and dirty limits. Based on this discussion we propose a semiempirical interpolation formula for $Q(T=0)$ which is also valid for compounds in between the dirty and clean limits. [S0163-1829(99)00806-1]

I. INTRODUCTION

One of the great challenges in the research of high-T_c superconductors (HTS's) is the understanding of vortex motion which is responsible for the occurrence of resistivity below T_c in HTS's in presence of a magnetic field. For technological applications the decay of the superconducting current is disastrous and here the main question is how to reduce the movement of vortices. But scientifically speaking vortices in motion supply an ideal physical laboratory system, both from the theoretical and experimental point of view: the number of vortices and their mutual interaction can be varied by the external magnetic field B_e, the resulting vortex lattice interacts with the crystal lattice of the host material and its defects and the amount of vortex motion is directly related to the temperature T. As a result of the interplay between these parameters the vortex system in HTS's possesses an intricate B_e-T phase diagram, which can be studied in great detail by independently varying B_e, T, the host material and its defect structure while measuring the dissipation with various methods.

Thus it was found soon after the discovery of HTS's that a superconducting current decay occurred even at very low temperatures (typically below 1 K), much larger than expected solely on the basis of thermally activated vortex motion.[1] It has been proposed that quantum tunneling of vortex segments, also called quantum creep, is responsible for such an anomalous residual relaxation at low temperatures. In case of the archetypal HTS $YBa_2Cu_3O_7$ the tunneling vortex segment has a length $L_c(0)\approx 1.3$ nm and a radius of the order of the coherence length $\xi_{ab}(0)\approx 1.6$ nm so that relative to the constituent electrons the tunneling segment is an almost macroscopic object. Theoretically quantum tunneling of a macroscopic object, i.e., an object which has (dissipative) interaction with its environment during tunneling, had already been studied extensively[2] and Caldeira and

Leggett[3(b)] proposed several conditions which a system has to satisfy before quantum tunneling of a large object can possibly be observed. Indeed these conditions are fulfilled for the vortex system in HTS's.

(i) Material defects in the HTS's like oxygen deficiencies, twin boundaries, or artificially introduced columnar defects provide potential wells for the vortices. In presence of a superconducting current density j_s a Lorentz force is exerted on the vortices, which effectively tilts the potential landscape and the pinning wells become metastable, local minima. Thus the activation energy barrier $U(j_s, T=0)$ decreases with increasing current and for current densities normally used in standard experiments it is experimentally found to be $\sim$25 K for $YBa_2Cu_3O_7$, although the pinning energy barrier U_0 $(T=0)(\equiv U[j_s=0, T=0])$ is as high as $\sim$150 K.

(ii) The lifetime of the metastable state t_m of a vortex segment as it would be in absence of the interaction with the environment should not be unobservably long, since this interaction will only further suppress tunneling. For the relevant case of a cubic pinning potential well of the form $U_{\rm pin}(x)=3U_0(x/x_0)^2(1-2x/3x_0)$ the lifetime is given by $t_m \approx 0.12(\hbar\omega_0/U)^{1/2}\omega_0^{-1}\exp(7.2U/\hbar\omega_0)$ [Ref. 3(c)] where x_0 is the range of $U_{\rm pin}(x)$ and ω_0 the frequency of oscillations of a vortex segment around its equilibrium position (also called attempt or trial frequency). For $YBa_2Cu_3O_7$ $\omega_0 \cong 10^{12}$ Hz,[4] fairly bigger than for conventional superconductors due to stronger pinning, leading to $t_m \sim 5\times10^{-4}$ s which is relatively short.

(iii) The quantum tunneling chance of a vortex segment without environmental interaction $\propto\exp(-U/\hbar\omega_0)$ [Ref. 3(c)] is bigger than the chance of thermal activation $\propto\exp(-U/k_BT)$ for $T\leqslant 10$ K in case of $YBa_2Cu_3O_7$ since then $k_BT\leqslant\hbar\omega_0$. But due to the interaction of the vortices with their environment the tunneling exponent increases. Therefore vortex motion will be unambiguously due to quantum tunneling rather than thermal activation typically for $T \leqslant 1$ K. Experimentally this temperature is still attainable.

(iv) Vortex tunneling can be directly registered and described in terms of resistivity ρ or current decay $\partial j_s/\partial t$, which are purely classical and macroscopic quantities. Finally, there is the advantage that the activation barrier height U can be varied experimentally by varying j_s as mentioned above. Therefore vortices in HTS's are considered as one of the few systems presently known[5] in which the intriguing phenomenon of macroscopic quantum tunneling can be observed.

Based on these considerations we performed measurements of the normalized relaxation rate $Q(T,B_e)$ of superconducting currents for temperatures T down to 100 mK in magnetic fields up to 7 T on various HTS's, using high sensitivity torque magnetometry.[6] As shown in a previous paper[7] the examined compounds—a $YBa_2Cu_3O_{7-\delta}$ thin film, a $YBa_2Cu_3O_{7-\delta}$ single crystal, a $YBa_2Cu_4O_8$ thin film, a $Tl_2Ba_2CaCu_2O_8$ thin film, a $Tl_2Ba_2Ca_2Cu_3O_{10}$ film and two $Pr_{1.85}Ce_{0.15}CuO_{4+\delta}$ single crystals with different oxygen doping[8]—represent two classes of materials, namely clean and dirty HTS's. This provides the opportunity to discuss the measurements in the context of the theoretical models for quantum creep in the clean and dirty limits.

In Sec. II we describe the experimental method used to determine $Q(T,B_e)$ for $T\geqslant 0.1$ K and $0\leqslant B_e\leqslant 7$ T, together with the precautions taken to provide good cooling of the sample. The resulting Q vs T curves are presented and their most interesting characteristics are summarized. In Sec. II we demonstrate that under the right experimental conditions unwanted local heating of the sample due to vortex motion can be avoided. Therefore, the generated heat is not at the origin of the observed finite $Q(T=0)$ and self-heating does not necessarily prohibit the observation of quantum creep[9] as has been suggested elsewhere.[10] We also prove that the residual value $Q(T=0)$ cannot be attributed to thermal activation down to very low T due to a distribution of pinning energy barriers. In Sec. IV the various characteristics of the Q vs T curves are discussed. For that purpose expressions for $Q(T)$ are derived in the thermal, crossover, and quantum regime ($T\gg 0$, $T\to 0$, and $T=0$, respectively). In contrast to the quadratic temperature dependence predicted theoretically, we unexpectedly find a linear temperature dependence of Q in the crossover regime between thermal activation and quantum tunneling above $B_e\cong 0.5$ T as a general feature of the investigated samples. Possible causes of this linear T dependence are discussed. We also demonstrate that an essential qualitative difference exists between the magnetic field dependence of Q in HTS thin films and single crystals, which is attributed to the presence of distinct pinning mechanisms in films and crystals. After determining the vortex regime of interest, the material dependence of quantum creep is subsequently treated. A semiemperical interpolation formula for $Q(T=0)$ is proposed for compounds in between the dirty and clean limits. Finally, conclusions are drawn in Sec. V.

II. EXPERIMENTAL METHOD AND RESULTS

A. Relaxation measured by torque

Due to vortex motion an electric field is induced in a type-II superconductor, effectively causing the superconducting current density j_s to pass through the normal vortex cores. Thus resistivity can be observed in HTS's below T_c. In case of thermal activation the induced electric field is given by the Lorentz expression

$$E=|\mathbf{B}_e\times\boldsymbol{\nu}|=\nu_0 B_e P_{ta} \tag{1}$$

with ν_0 the average vortex velocity between pinning sites and P_{ta} the chance of thermal activation of the vortex. The induced electric field is also described by Faraday's induction law

$$E(r)=-\frac{\Lambda(r)D}{2\pi}\frac{\partial j_s}{\partial t}-\frac{r}{2}\frac{dB_e}{dt} \tag{2}$$

with r the distance to the center of the sample which has effective radius R, thickness D, and self inductance $\Lambda \approx \mu_0 r\ln(r/D)$. Combining Eqs. (1) and (2) leads to the flux creep equation

$$\frac{\partial j_s}{\partial t}=-\frac{2\pi\nu_0 B_e}{\Lambda(R)D}P_{ta}+\frac{\pi R}{\Lambda(R)D}\frac{dB_e}{dt}, \tag{3}$$

describing the time decay of j_s in presence of vortex motion and changing B_e. In case of an effective activation energy $U(j_s,T,B_e)$, P_{ta} is given by

$$P_{ta}=\exp\left(-\frac{U(j_s,T,B_e)}{k_BT}\right) \tag{4}$$

following a Boltzmann statistic. Once the activation energy $U(j_s,T,B_e)$ is known, $j_s(T,B_e,t,\dot{B}_e)$ can be solved from Eq. (3). For thermally activated vortex motion $U(j_s,T,B_e)$ can be very generally parametrized in the form[11,12]

$$U(j_s,T,B_e)=U_0(T,B_e)f(j_s), \tag{5}$$

where the function $f(j_s,T,B_e)$ is given by

$$f(j_s)=\frac{1}{\mu(T,B_e)}\left[\left(\frac{j_c(T,B_e)}{j_s(T,B_e)}\right)^{\mu(T,B_e)}-1\right], \tag{6}$$

with μ the only parameter which influences the current dependence of U, and j_c the critical current density for which $U(j_s)$ vanishes. Note that the Kim-Anderson model is obtained for $\mu=-1$, that one finds the Zeldov logarithmic model for $\mu=0$ and that various weak collective pinning models are characterized by $\mu>0$. Vice versa, measuring j_s as function of time t or sweep rate $\dot{B}_e$ at various T and B_e provides the opportunity to determine $U(j_s,T,B_e)$ and thus to gain insight in the process of vortex pinning.

Therefore we perform two types of relaxation experiment. In a conventional relaxation the normalized relaxation rate $S\equiv-\partial\ln j_s/\partial\ln t$ is measured by observing the time decay of j_s after stopping the magnetic field sweep at the field of interest. For this type of experiment the second term on the right-hand side (rhs) of the flux creep Eq. (3) therefore vanishes and using Eqs. (5) and (6) yields

$$S\approx\frac{k_BT}{U_0}\left(\frac{j_s}{j_c}\right)^{\mu}, \tag{7}$$

where S should be evaluated for time intervals typically starting 10 s after the start of the relaxation. In a dynamic relaxation experiment the normalized relaxation rate $Q\equiv\partial\ln j_s/\partial\ln\dot{B}_e$ is determined by performing hysteresis loops at various sweep rates $\dot{B}_e$ around the field of interest.[13] In this type of experiment B_e is swept continuously typically with $\dot{B}_e\geqslant 1$ mT/s and here the left-hand side (lhs) of Eq. (3) can be neglected with respect to the second term on the rhs. Using Eqs. (5) and (6) then yields

$$Q=\frac{k_BT}{U_0}\left(\frac{j_s}{j_c}\right)^{\mu}. \tag{8}$$

The dynamic relaxation rate $Q(T,B_e)$ therefore is essentially the same as the conventional relaxation rate $S(T,B_e)$ for activation energies of the form of Eq. (5).

In our experiments j_s is solely induced by the inhomogeneity of the vortex distribution inside the sample due to pinning (i.e., $\nabla\times\mathbf{B}=\mu_0\mathbf{j}_s$). The magnetic moment M corresponding to j_s can directly be monitored using the torque $\boldsymbol{\tau}=\mathbf{M}\times\mathbf{B}_e$. In our case a sample is always mounted with an angle of 20° between its c axis and $\mathbf{B}_e$, large enough to have an appreciable torque but small enough to allow the approximation $\mathbf{B}_e\|\hat{z}$. We determine τ by capacitively measuring the displacement of a spring to which the sample is attached (see Fig. 1). This displacement is proportional to τ for small deflections.[6] The capacitance C is typically of the order of 1 pF and is determined with a capacitance bridge (General Radio 1615-A) in combination with a lock-in amplifier (PAR 128A). Thus torque magnetometry is well suited for use in the mK regime since the dissipated power is typically of the order $\frac{1}{2}CV_0^2\leqslant 5$ nW for an ac excitation voltage amplitude $V_0\leqslant 100$ V. The torque meter is calibrated by mounting a small coil at the place of the sample to produce a known magnetic moment. Assuming a homogeneous current distribution throughout the sample, j_s can be calculated using $M=\Omega j_s$ with $\Omega=(\frac{1}{4})W^2D(L-W/3)$ for a rectangular sample with length L and width W ($W\leqslant L$) and $\Omega=(\pi/3)D(R_{\rm out}^3-R_{\rm in}^3)$ for a ring-shaped sample. The external magnetic field B_e is supplied by an Oxford Instruments 7 T superconducting magnet.

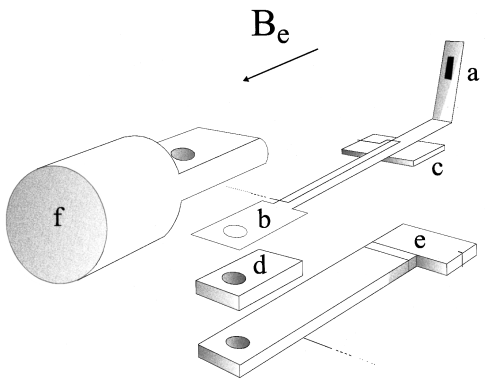

FIG. 1. Schematic drawing of a torque meter designed to measure the superconducting current density j_s of small crystals in a dilution refrigerator. The sample (a) is cooled by heat conduction via a gold covered spring (b). The spring, to which a capacitance plate (c) is attached, is clamped together with a spacer (d) and a second capacitance plate (e) to the tail of the refrigerator (f) by a bolt and nut.

B. Optimization of cooling

Since in our dilution refrigerator (Oxford Instruments Kelvinox dilution refrigerator, 20 μW cooling power at 0.1 K) the sample is suspended in vacuum, heat conduction is only possible by way of the torque meter on which the sample is mounted. The cooling has therefore been optimized as follows. The thin films are c-axis grown on top of an insulating $SrTiO_3$ or $LaAlO_3$ substrate. A 500-nm-thick silver layer is deposited on the thin films using a finger-shaped mask to avoid eddy currents in the silver during field ramping. Then one end of a pure copper foil (dimensions $15\times5\times0.01\,\mathrm{mm}^3$) is indium soldered to the silver layer, while the other end is tightly clamped to the copper tail of the dilution refrigerator. An applied field of less than 0.03 T suffices to turn the indium [$T_c=3.4$ K, $B_c(T=0)=0.0293$ T] normal. The sandwich of substrate, thin film, and silver layer is mounted on the plastic holder of a torque meter by Teflon tape. Except for the sample and this plastic

holder all parts of the torque meter are mounted parallel to the magnetic field so that eddy current heating is negligible. In this way the temperature difference between the refrigerator tail (which now stands for the cold bath) and the sample is estimated to be maximally 5 mK under typical measurement conditions at $T_b = 0.1$ K and it can be neglected above $T_b = 0.15$ K. The single crystals are mounted with a thin layer of N Apiezon grease (thickness about 1 μm) on the phosphor-bronze spring (dimensions $13 \times 0.5 \times 0.1$ mm^3) of the torque meter. This spring has first been covered electrolytically with a 20-μm-thick gold layer and is tightly clamped with one end to the tail of the dilution refrigerator. The sample is mounted at the other end of the spring and here only a piece of 3 mm length is pointing into the magnetic field so that eddy current heating is negligible (see Fig. 1). The Kapitza resistance R_K is expected to play a role only in case of the single crystals where N Apiezon grease has been used. Assuming that the gold-grease and sample-grease contacts lead to Kapitza resistivities of the order of $r_K(T) \sim 10^{-3}/T^3$ K m^2/W as found for copper-grease contacts,[14] the temperature difference between the cold bath and the sample in this case can be estimated to be maximally 5 mK under typical experimental conditions at $T_b = 0.1$ K. Above $T_b = 0.15$ K this temperature difference again is negligible. To test the cooling we measured the reversible torque signal of an aluminium disc ($T_c = 1.14$ K, $R = 2.5$ mm, $D = 2$ mm) attached with the first method, but using N Apiezon grease instead of a silver overlayer and indium soldering. With $B_c(T=0) = 10.5$ mT (Ref. 15) we find that the measured value $B_c(T_b = 0.1\,\text{K}) \approx 10.4 \pm 0.3$ mT corresponds to $T \approx 0.11 \pm 0.10$ K for the sample using the empirical relation $B_c(T) = B_c(0)[1-(T/T_c)^2]$. The main cause of the great uncertainty in T is the ambiguity in determining B_c, but the value found indicates that the cooling is satisfactory and that the temperature inside the sample compares well to T_b even at the lowest temperatures where heating effects are largest. T_b is measured using a calibrated carbon resistor (Leiden Cryogenics) attached to the mixing chamber of the dilution refrigerator, in combination with a low-dissipation resistance bridge (RV-Elektroniikka AVS-47).

C. Results

Typical results obtained from dynamic relaxation measurements are shown in Fig. 2 for a $YBa_2Cu_3O_{7-\delta}$ ring-shaped thin film at $T = 99 \pm 1$ mK. $Q \equiv \partial \ln j_s / \partial \ln \dot{B}_e$ can be determined as the slope of the $\ln j_s$ vs $\ln \dot{B}_e$ curves (see inset of Fig. 2). The constant slope of these curves is an indication of the absence of self-heating for $\dot{B}_e$ as high as 40 mT/s. Self-heating would cause an increasing internal temperature for higher sweep rates and would therefore lead to a negative curvature of the $\ln j_s$ vs $\ln \dot{B}_e$ curves. On the contrary, according to vortex glass (VG) theory[16] this curvature should be zero or positive. Since $E \propto \dot{B}_e$ (e.g., for the ring-shaped $YBa_2Cu_3O_{7-\delta}$ thin film $\dot{B}_e = 5$ mT/s corresponds to an induced electric field $E = (R/2\dot{B}_e) = 2 \times 10^{-5}$ V/m) the $\ln j_s$ vs $\ln \dot{B}_e$ curves can be converted to $\ln E$ vs $\ln j_s$ plots (or I-V plots). In the low-E and high-j_s regime at low T the vortex system is predicted to be in a glass phase characterized by an exponential decrease of E with decreasing j_s. The $\ln E$ vs $\ln j_s$ plots should therefore be linear or have negative curvature when approaching the melting line, which corresponds to a zero or positive curvature of the $\ln j_s$ vs $\ln \dot{B}_e$ curves.

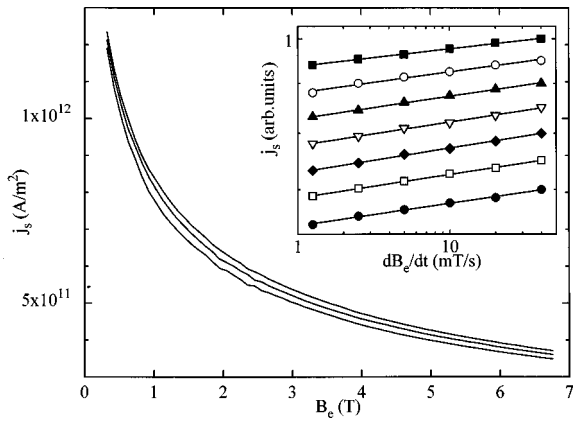

FIG. 2. Superconducting current density j_s vs B_e for a $YBa_2Cu_3O_{7-\delta}$ thin film at $T = 99 \pm 1$ mK measured at various sweep rates. From top to bottom: $dB_e/dt = 20$, 5, and 1.25 mT/s (the curves for 40, 10, and 2.5 mT/s are not shown). In the inset: the corresponding $\ln j_s$ vs $\ln dB_e/dt$ curves from which $Q \equiv \partial \ln j_s / \partial \ln dB_e/dt$ can be determined. From top to bottom: $B_e = 0.5$, 1, 2, 3, 4, 5, and 6 T. The curves are shifted for clarity by multiplying them with an arbitrary number.

Typical conventional relaxation measurements are shown in Fig. 3 for a $Pr_{1.85}Ce_{0.15}CuO_{4+\delta}$ single crystal ($T_c = 23.2$ K) at $T = 101 \pm 1$ mK where $S \equiv -\partial \ln j_s / \partial \ln t$ can be determined directly from the slope of the curves. Here the almost perfect logarithmic time decay, predicted by VG theory for vortices in the glass phase, is indicative for temperature stability and the absence of self-heating. The low signal-to-noise ratio for small B_e is due to the insensitivity of torque when $B_e \to 0$, the rapid growth of the noise level with increasing B_e is caused by the exponential decay $j_s \propto \exp -B_e$ which we find for $Pr_{1.85}Ce_{0.15}CuO_{4+\delta}$.

Although dynamic and conventional relaxation are experimentally very different methods, they provide fundamentally the same information about vortex motion. A general analysis of the flux creep equation[17] leads to

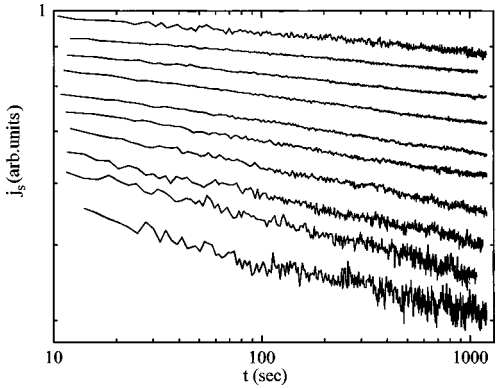

FIG. 3. $\ln j_s$ vs $\ln t$ for a $Pr_{1.85}Ce_{0.15}CuO_{4+\delta}$ single crystal ($T_c = 23.2$ K) at $T = 101 \pm 1$ mK from which $S \equiv -\partial \ln j_s / \partial \ln t$ can be determined. From top to bottom: $B_e = 0.1$, 0.5, 1, 2, 3, 4, 4.5, 5.5, 6, and 6.5 T. The curves are shifted for clarity by multiplying j_s with an arbitrary number.

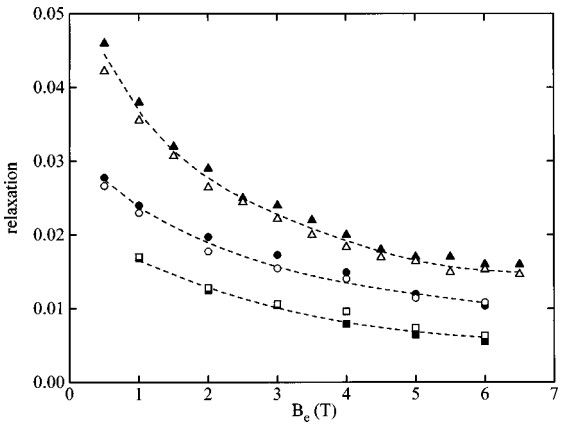

FIG. 4. Comparison between dynamic relaxation rate $Q \equiv \partial \ln j_s / \partial \ln \partial B_e / \partial t$ and conventional relaxation rate $S \equiv -\partial \ln j_s / \partial \ln t$ (solid and open symbols, respectively) for a $YBa_2Cu_3O_{7-\delta}$ single crystal at $T=3$ K (triangles), 1 K (circles), and 0.1 K (squares). Dashed lines are guides to the eye.

$$Q = S\left(1 - \frac{\dot{B}_e \dfrac{\partial}{\partial \dot{B}_e}(\partial j_s/\partial B_e)}{\chi/\mu_0\Omega - \partial j_s/\partial B_e}\right) \tag{9}$$

with $\chi = LWD$ for a rectangular sample, $\chi = [\pi^2/3\ln(R_{\rm out}/D)](R_{\rm in}^3 - R_{\rm out}^3)$ for a ring-shaped sample and where S should be evaluated typically for $t > 10$ s after the start of the conventional relaxation. Experimentally $\partial j_s/\partial B_e$ is found to be independent of $\dot{B}_e$ for the sweep rates used (as can be seen, e.g., in Fig. 2) and therefore Q and S are expected to be equivalent. In Fig. 4 we show that indeed this is true for values of Q and S measured at low T for the $YBa_2Cu_3O_{7-\delta}$ single crystal. This also provides an additional indication of the good quality of the cooling, since the extra heat generated in a fast dynamic relaxation measurement would otherwise have led to $Q(T,B_e) > S(T,B_e)$ at low T. In the succeeding sections we will not distinguish between Q and S any more and denote both quantities by Q, stressing the quantum mechanical origin of the finite values of dynamic or conventional relaxation which we find for $T \to 0$.

In Figs. 5(a)–5(f) the measured Q vs T curves are shown for various HTS's in the temperature range $0.1 \leqslant T \leqslant 4.5$ K for B_e up to 7 T. Clearly the curves do not extrapolate to $Q(T=0)=0$ which is a clear evidence for quantum creep in these materials. We point out some characteristics.

First, the theoretically unexpected linear temperature dependence $Q(T) = Q(0) + aT$ of quantum creep which we first reported for the $YBa_2Cu_3O_{7-\delta}$ and $YBa_2Cu_4O_8$ thin films[18] and which has been emphasized by Seidler *et al.*,[19] is a general feature at high fields for all the samples investigated here. Only at low fields for the $Tl_2Ba_2CaCu_2O_8$ thin film [Fig. 5(d)], the $Tl_2Ba_2Ca_2Cu_3O_{10}$ film and the $Pr_{1.85}Ce_{0.15}CuO_{4+\delta}$ single crystal with $T_c = 12.1$ K [Fig. 5(f)] the theoretically expected quadratic T dependence is observed at low fields in the crossover regime between thermally activated and quantum motion, but turns into a linear T dependence at higher fields. Since the samples are magnetically fully penetrated before every relaxation measurement (by first sweeping B_e over an appropriate interval) and since any background has been corrected (for instance a paramagnetic background in case of the $Pr_{1.85}Ce_{0.15}CuO_{4+\delta}$ samples) we are convinced that this characteristic is not a measurement artefact, but a striking physical phenomenon.

Second, the magnetic field dependence of quantum creep is very different for a single crystal and a thin film of the same compound [in this case of $YBa_2Cu_3O_{7-\delta}$, Figs. 5(a) and 5(b), respectively], although the $Q(T)$ curves are very similar. At fixed T, Q decreases and saturates with increasing field for the single crystal while it increases and saturates at the same value with increasing field for the thin film, which is the general magnetic field behavior of the films investigated here.

Third, the extrapolated $Q(T=0)$ values are very similar and close to 0.02 for all the examined compounds for $B_e \geqslant 1$ T except for the $Pr_{1.85}Ce_{0.15}CuO_{4+\delta}$ single crystals which have significantly higher $Q(T=0)$. From the point of view of vortex dynamics the latter samples therefore seem to belong to a different class of materials.

But before discussing these characteristics in Sec. IV, we now first prove in Sec. III that heating effects can be excluded as the cause of the observed residual relaxation for $T \to 0$ K.

III. EXCLUDING THERMAL EFFECTS FOR $T \to 0$

It has been argued[10] that *under adiabatic conditions* the dissipation associated with the movement of vortices leads to a rise of the temperature in the sample. It is obvious that even vortex avalanches can be provoked due to self-heating when adiabatic conditions are approached in a sample with low thermal conductivity by reducing the thermal contact of the sample with the cold bath and increasing the generated power for instance by maximizing the magnetic-field sweep rate. But we now show that by minimizing the self-heating the low temperatures necessary to distinguish quantum creep can be reached within the thin films and crystals of the HTS's examined in this work. We also prove that thermal activation down to very low T in a system with a finite density of vanishingly small activation energies cannot explain the observed finite $Q(T=0)$.

A. Self-heating due to vortex motion

The power p generated inside a HTS due to dissipation in the normal vortex cores can be estimated by

$$p = \int_V j_s E(r) d^3r = 2\pi D j_s \int_0^R E(r) r dr \tag{10}$$

assuming that j_s is homogeneous throughout the sample with volume V and where $E(r)$ is given by Eq. (2). In a conventional relaxation experiment the second term on the rhs of Eq. (2) vanishes and Eq. (10) yields

$$p_S = \frac{\mu_0 D^2 R^3}{9}\left(3\ln\frac{R}{D} - 1\right)\left.\frac{\partial j_s}{\partial t}\right|_{T,B_e,t} j_s(T,B_e,t). \tag{11}$$

In a dynamic relaxation experiment the first term on the rhs of Eq. (2) can be neglected with respect to the second. In this case Eq. (10) therefore yields

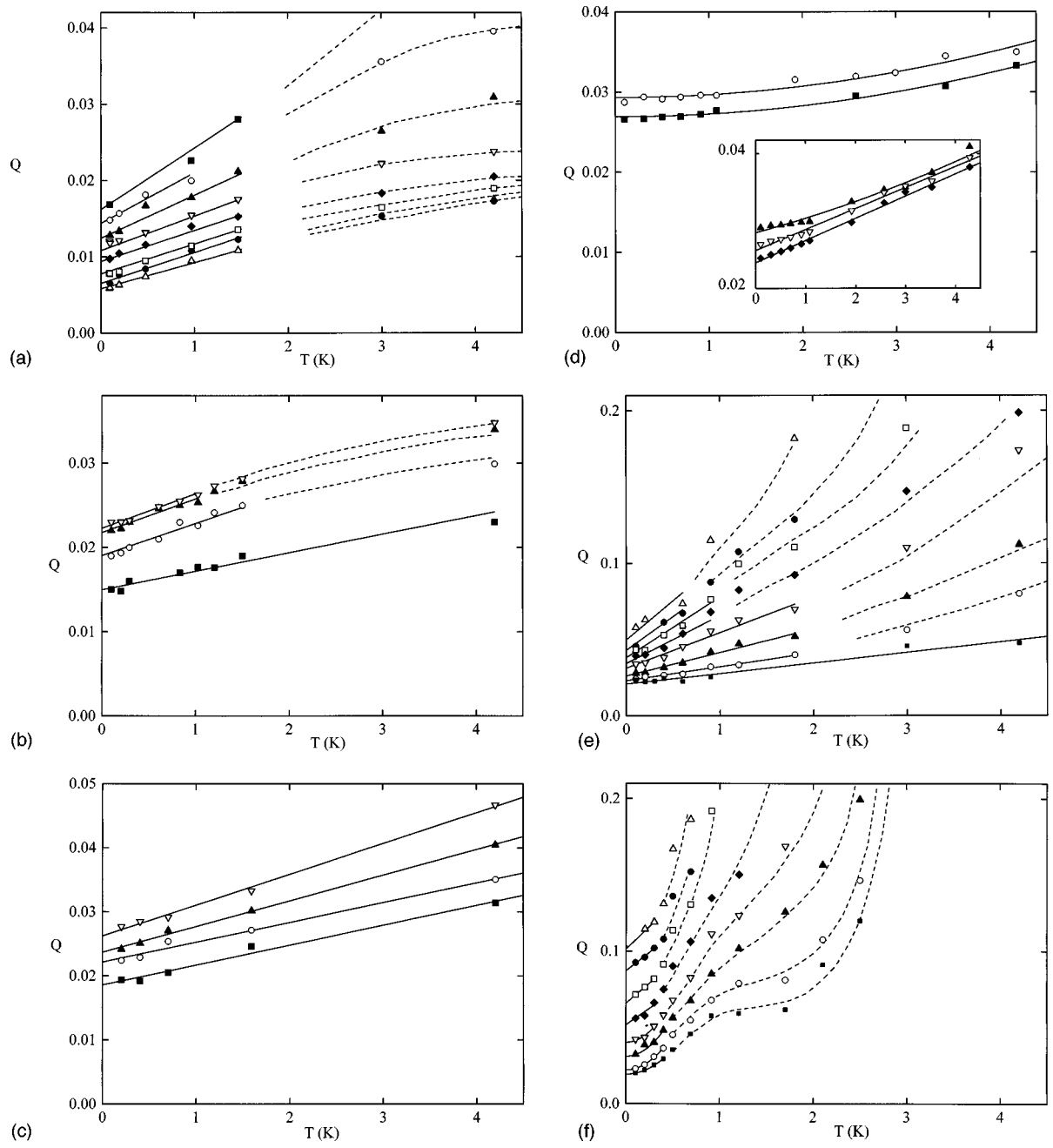

FIG. 5. (a) Q vs T for the $YBa_2Cu_3O_{7-\delta}$ single crystal. Solid lines are the appropriate fits in the crossover regime from which $Q(T=0)$ is determined. Dashed lines are guides to the eye. From top to bottom: $B_e=0.3$, 1, 2, 3, 4, 5, 6, and 7 T. (b) Q versus T for the $YBa_2Cu_3O_{7-\delta}$ thin film. From top to bottom: $B_e=3$, 2, 1, and 0.5 T. For $B_e \geqslant 3$ T the $Q(T)$ curves coincide and only the curve at $B_e=3$ T is plotted for clarity. (c) Q vs T for the $YBa_2Cu_4O_8$ thin film. From top to bottom: $B_e=6$, 5, 3, and 1 T. (d) Q versus T for the $Tl_2Ba_2CaCu_2O_8$ thin film for $B_e=0.5$ T (full squares) and $B_e=1$ T (open circles). In the inset: $B_e=6$, 4, and 2 T from top to bottom. (e) Q vs T for the $Pr_{1.85}Ce_{0.15}CuO_{4+\delta}$ single crystal ($T_c=23.2$ K). From top to bottom: $B_e=6$, 5, 4, 3, 2, 1, 0.5, and 0.1 T. (f) Q vs T for the $Pr_{1.85}Ce_{0.15}CuO_{4+\delta}$ single crystal ($T_c=12.1$ K). From top to bottom: $B_e=2.5$, 2, 1.5, 1, 0.6, 0.4, 0.2, and 0.1 T.

$$p_Q=\frac{\pi R^3 D}{3}\frac{dB_e}{dt}j_s(T,B_e,\dot{B}_e). \tag{12}$$

Assuming p is generated homogeneously throughout the sample, the temperature T_i inside the sample during the different experiments can now be calculated by solving the heat transport equation for a sample in a stationary state

$$(1-z/D)p=\kappa(T)A\frac{dT}{dz}, \tag{13}$$

where z is the distance to the surface which is in contact with the cold bath at temperature T_b, A the cross-sectional area through which the heat is transported, and $\kappa(T)$ the thermal conductivity of the sample. Integration leads to

$$T_i(T_b,z)=\left(T_b^4+\frac{4z(1-z/2D)p}{\alpha A}\right)^{1/4} \tag{14}$$

in case of a thermal conductivity dominated at low T by surface scattering of phonons with $\kappa(T)=\alpha T^3$. For other

TABLE I. Parameters of the high-T_c samples considered in this work, necessary to estimate the temperature T_i at position $z=D$ furthest from the sample surface which is in contact with the cold bath at temperature $T_b=100$ mK. L, W, and D are length, width, and thickness of the samples. For the rings L is the outer radius and W the width of the ring. $\kappa_c(T)$ is an estimated underlimit for the c-axis thermal conductivity, p_Q the total power typically generated in a hysteresis loop experiment [see Eq. (12)], and p_S the total power typically generated in a conventional relaxation experiment [see Eq. (11)]. Values of j_s are at $T=0.1$ K, $B_e=1$ T (0.01 T for $Tl_2Ba_2Ca_2Cu_3O_{10}$), and $\dot{B}_e=5$ mT/s in case of dynamic relaxation, values of $\partial j_s/\partial t$ and j_s are at $T=0.1$ K, $B_e=1$ T, and $t=10$ s after the start of a conventional relaxation.

Dynamic relaxation	L (mm)	W (mm)	D (μm)	$\kappa_c(T)$ (mW/Km)	dB_e/dt (mT/s)	j_s (A/m^2)	p_Q (μW)	$T_i(D)$ (mK)
$YBa_2Cu_3O_{7-\delta}$ film (ring)	4	0.5	0.180	$60\times T^3$	5	8×10^{10}	1.6	100
$YBa_2Cu_4O_8$ film	5	3.5	0.200	$120\times T^3$	5	1×10^{11}	1.4	100
$Tl_2Ba_2CaCu_2O_8$ film (ring)	1.5	1.475	0.200	$1.25\times T^{2.5}$	5	8×10^{11}	0.14	113
$Tl_2Ba_2Ca_2Cu_3O_{10}$ film	4	3	1	$1.25\times T^{2.5}$	5	3.9×10^{10}	1.5	114
$Pr_{1.85}Ce_{0.15}CuO_{4+\delta}$ single crystal ($T_c=12.1$ K)	1.38	0.92	40	$7.5\times T^2$	5	1×10^9	0.05	110
Conventional relaxation	L (mm)	W (mm)	D (μm)	κ_c(T) (mW/Km)	$\partial j_s/\partial t$ (A/m^2 t)	j_s (A/m^2)	p_S (nW)	$T_i(D)$ (mK)
$YBa_2Cu_3O_{7-\delta}$ single crystal	1.69	0.34	10	$60\times T^3$	3×10^7	7.5×10^9	2.5	100
$Pr_{1.85}Ce_{0.15}CuO_{4+\delta}$ single crystal ($T_c=23.2$ K)	1.36	0.9	15	$7.5\times T^2$	1.2×10^7	5.7×10^9	5.4	100

temperature dependencies of $\kappa(T)$ a similar expression is found. For the examined compounds we summarize in Table I the calculated T_i at $T_b=0.1$ K and $z=D$, furthest from the cooled surface of the sample, under typical experimental conditions. To our knowledge, of this set of materials, $\kappa(T)$ has only been measured in the milli-Kelvin regime for a $YBa_2Cu_3O_{7-\delta}$ single crystal[20] and for related materials like ceramic $Tl_2Ba_2Ca_2Cu_3O_{10}$ (Ref. 21) and ceramic $Nd_{1.85}Ce_{0.15}CuO_{4+\delta}$.[22] Therefore, we assume $\kappa(YBa_2Cu_4O_8)\approx2\kappa(YBa_2Cu_3O_{7-\delta})$,[23] $\kappa(Tl_2Ba_2CaCu_2O_8)\approx\kappa(Tl_2Ba_2Ca_2Cu_3O_{10})$,[24] and $\kappa(Pr_{1.85}Ce_{0.15}CuO_{4+\delta})\approx0.5\kappa(Nd_{1.85}Ce_{0.15}CuO_{4+\delta})$ (Ref. 25) as found for $T\geq10$ K and $\kappa_c\approx0.5\,\kappa_{ab}$ as found for $YBa_2Cu_3O_{7-\delta}$ in the milli-Kelvin range.[20] Since the latter sample is almost cubic, the anisotropy κ_c/κ_{ab} reflects the small difference in, e.g., the oscillator strengths in the different directions. We then assume this small inherent anisotropy to be general for our samples. The values of κ_c thus found will be underlimits for our thin films, since here the cooling surface is much larger than for the samples in Refs. 20–25. For the $YBa_2Cu_3O_{7-\delta}$ single crystal the calculated temperature profile within the sample is plotted in Fig. 6 for a hysteresis loop experiment with $\dot{B}_e=5$ mT/s. Above $T_b=0.13$ K dissipation leads to $T_i(D)$ within 1% of T_b which is better than the temperature stability and self-heating can be neglected. Self-heating begins to play a minor role at $T_b=0.1$ K where $T_i(D)=0.104$ K. $T_i(D)$ starts to saturate around $T_b=0.075$ K and has a residual value of 0.064 K for $T_b\rightarrow0$. If one wishes to diminish this residual value and the temperature for which saturation sets in, one can use lower sweep rates and perform conventional relaxation experiments with low intermediate field ramp rate (see Table I). In the $YBa_2Cu_3O_{7-\delta}$ thin film the problem is much less and $\dot{B}_e=5$ mT/s leads to negligible self-heating above $T_b=0.06$ K, saturation of $T_i(D)$ around $T_b=0.04$ K and a residual value $T_i(D)=0.03$ K for $T_b\rightarrow0$. For the thin films we therefore performed dynamic relaxation experiments thus avoiding magnetic-field overshoot when stopping a field sweep, which has great effect on the conventional relaxation process for samples with small penetration field B_p.[26] For the single crystals with high B_p the overshoot effect is small and here we performed conventional relaxation measurements to reduce self-heating (except for the $Pr_{1.85}Ce_{0.15}CuO_{4+\delta}$ single crystal with $T_c=12.1$ K which only supports low j_s).

B. Distribution of activation energies

When a distribution of pinning energies $m(U_0)$ exists in the sample one could expect at first sight that thermal activation from the most shallow pinning wells even occurs for $T\rightarrow0$, resulting in a finite extrapolated $Q(T=0)$. Let us therefore consider this case in more detail and define an energy distribution function such that $\int_0^\infty m(U_0)dU_0=1$. Instead of Eq. (4) the chance for thermal activation now becomes

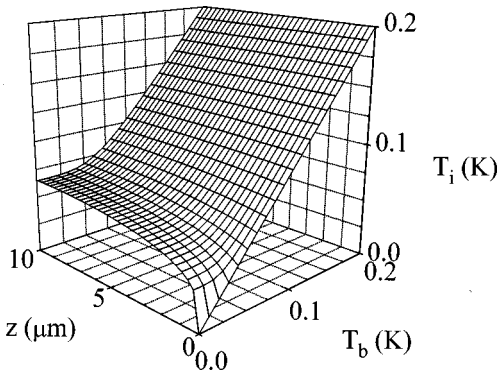

FIG. 6. Temperature T_i inside the $YBa_2Cu_3O_{7-\delta}$ single crystal as function of the temperature T_b of the surface which is in contact with the cold bath and the position z relative to this surface, calculated for a hysteresis loop experiment using Eqs. (12) and (14). Dimensions of the crystal: $L\times W\times D=1.69\times0.34\times0.01$ mm^3, magnetic-field sweep rate: $dB_e/dt=5$ mT/s, $j_s(T\sim0.1\,\mathrm{K}, B_e=1\,\mathrm{T}, dB_e/dt=5\,\mathrm{mT/s})=8\times10^9$ A/m^2. Note that above 0.1 K the temperature in the sample is essentially equal to that of the bath.

$$P_{ta}=\int_0^\infty \exp[-U_0 f(j_s)/k_B T]m(U_0)dU_0, \qquad (15)$$

which can be used to evaluate the flux creep Eq. (3). For a dynamic relaxation experiment the lhs of Eq. (3) can be neglected with respect to the second term on the rhs and the flux creep equation becomes

$$P_{ta}=\frac{RdB_e/dt}{2\nu_0 B_e}\equiv \dot{b}. \qquad (16)$$

Since $\dot{b}$ is well defined the integral in Eq. (16) can be evaluated analytically or numerically for any $m(U_0)$, which gives

$$f(j_s)=k_B T G(\dot{b}) \qquad (17)$$

with G a function depending on $\dot{b}$ only and $f(j_s)$ given by Eq. (6). We subsequently take the logarithm of Eq. (17) and differentiate it with respect to $\ln T$ and $\ln \dot{b}$. Combining the two results finally yields

$$\frac{d\ln G}{d\ln \dot{b}}\,\frac{T}{j_s}\,\frac{\partial j_s}{\partial T}=\frac{\partial \ln j_s}{\partial \ln \dot{b}}=\frac{\partial \ln j_s}{\partial \ln \dot{B}_e}\equiv Q(T,B_e) \qquad (18)$$

with $Q(T,B_e)$ the dynamic relaxation rate. Since $\partial j_s/\partial T$ does not diverge when T approaches 0 K and $d\ln G/d\ln \dot{b}$ is finite, it follows immediately from Eq. (18) that also in the case of a distribution of pinning energies $Q(T,B_e)\to 0$ when $T\to 0$, if there is thermally activated motion only.

IV. DISCUSSION

A. Theoretical description of $Q(T)$

For the case of a quadratic effective pinning potential in one dimension $U_{\rm pin}(x)=U_0(x/x_0)^2$ which drops abruptly to a negative value at $x=x_0$, Caldeira and Leggett[3(d)] and Stephen[27] pointed out that the standard expression[28]

$$P\propto \exp-\frac{x_0^2}{2\langle x^2\rangle} \qquad (19)$$

for the probability of *nondissipative* motion out of the well leads to the correct expression for the tunneling probability also in case of *dissipative* tunneling as derived rigorously by Caldeira and Leggett,[3(a)] Larkin and Ovchinnikov,[29] Blatter *et al.*,[30] and Ao and Thouless.[31] Here $\langle x^2\rangle$ is the mean-square displacement of the vortex. The result from Eq. (19) and the exact result will only differ by a multiplicative factor in the exponent. Therefore we replace the number 2 in Eq. (19) by a general constant c, which can be determined experimentally or by comparison with the rigorous semiclassical expressions.

In presence of a superconducting current density j_s a Lorentz force $L_c\phi_0\mathbf{j}_s\times\hat{z}$ is exerted on a moving vortex segment with length L_c, where ϕ_0 is the flux quantum corresponding to one vortex. This Lorentz force is taken into account effectively by a current dependence of x_0. E.g., for a quadratic pinning potential, x_0 diminishes like $x_0(1-j_s/j_c)$ and fully vanishes at the critical current density j_c. However, instead of using a quadratic potential a cubic effective pinning potential $U_{\rm pin}(x)=3U_0(x/x_0)^2(1-2x/3x_0)$ would be more favorable since it is a good approximation of any realistic pinning barrier for $j_s\approx j_c$ (i.e., near criticality where x_0 vanishes), with U_0 and x_0 corresponding to the height and range of the real potential. Therefore, we will use Eq. (19) also in case of a cubic pinning barrier since close to the center such a pinning barrier can be well approximated by a quadratic potential. For a cubic pinning potential x_0 decreases like $x_0(1-j_s/j_c)^{1/2}$ and when P_{ta} is replaced in the flux creep equation [Eq. (3)] by the expression for P of Eq. (19) we find

$$Q=\frac{c\langle x^2\rangle}{x_0^2}\,\frac{j_c}{j_s} \qquad (20)$$

for the dynamic relaxation rate as well as for the conventional relaxation rate for t typically bigger than 10 s. The multiplicative factor c in the exponent of Eq. (19) explicitly appears while the factor before the exponential function can be disregarded, since it does not contribute to the relaxation rate [however, for a quantitative description of $j_s(T,B_e)$ it has to be incorporated explicitly]. Equation (20) is valid in the thermal, quantum and crossover regime since Eq. (19) is applicable over the full temperature range. It can be extended to three dimensions for a three-dimensional pinning potential $U_{\rm pin}(x,y)=U_0[3(x^2+y^2)/u_0^2-2(x^3+y^3)/u_0^3]$ with $x_0=y_0\equiv u_0$ and where x is in the direction of the Lorentz force, i.e., perpendicular to $\mathbf{j}_s$.

To obtain a semiclassical description of $Q(T)$ we therefore determine the mean-square displacement $\langle u^2\rangle$ from the equation of motion of a vortex in three dimensions:

$$m\ddot{\mathbf{u}}+k\mathbf{u}+\eta\dot{\mathbf{u}}+\alpha\hat{z}\times\dot{\mathbf{u}}=0. \qquad (21)$$

Here $\mathbf{u}$ is the displacement of the vortex, $k\mathbf{u}$ the pinning force corresponding to $U_{\rm pin}$ close to the center of the pinning well, and $m\approx k/\omega_0^2=2U_0/\omega_0^2x_0^2$ the mass of the moving vortex segment. The intra- and intervortex interaction can be included by a T and B_e dependence of k which then takes the line tension and mutual shear, tilt, and compression forces into account by adjusting the steepness of $U_{\rm pin}$. A field induced transition between pinning mechanisms can be accounted for in the same way. The size of the tunneling object and its mass will change accordingly.

The terms $\eta\dot{\mathbf{u}}$ and $\alpha\hat{z}\times\dot{\mathbf{u}}$ describe the interaction of the vortex with its host material via the electrons in the normal vortex core. This can be seen as follows: when a vortex moves, the local change in current density gives rise to a homogeneous electric field $\mathbf{E}=(\phi_0/2\pi\xi_{ab}^2)\hat{z}\times\dot{\mathbf{u}}\equiv B_{c2}\hat{z}\times\dot{\mathbf{u}}$ inside the vortex core. Alternatively the electric field can be interpreted as the result of the electrons, which have become normal in the vortex core, virtually being subject to a moving magnetic field with a magnitude as high as B_{c2} as the vortex passes by. In the electron frame of reference this would be equivalent to a magnetic field $\mathbf{B}_{c2}$ *and* an electric field $\mathbf{E}=B_{c2}\hat{z}\times\dot{\mathbf{u}}$. This electric field generates a current density $\mathbf{j}_{\rm core}$ in the normal core and thus dissipation occurs in the HTS. The force modeling the intricate interaction between the vortex and its host material has the Lorentz form

$$\mathbf{F}_{\rm int}=-L_c\phi_0\mathbf{j}_s\times\hat{z} \qquad (22)$$

since it must cancel the Lorentz force when the vortex is moving uniformly between pinning sites.[32] Here it is assumed, as in the standard Bardeen-Stephen theory for dissipation in vortices,[33] that the interaction only takes place within the moving volume with length L_c. However, as shown below, there exist materials in which dissipation extends beyond the volume of the moving vortex segment. In that case L_c in Eq. (22) has to be replaced by an effective length $L_{\rm eff}$ defined as the length of the volume in which dissipation takes place, with $L_{\rm eff}>L_c$. But let us continue for the moment to use the Bardeen-Stephen assumption $L_c = L_{\rm eff}$. Applying the well-known Drude relation

$$\mathbf{j}_{\rm core}=\frac{1}{1+(\omega_e\tau)^2}\frac{1}{\rho_n}(\mathbf{E}+\omega_e\tau\hat{z}\times\mathbf{E}) \tag{23}$$

in the normal core and assuming that the magnitude and direction of $\dot{\mathbf{u}}$ is such that $\mathbf{j}_{\rm core}=\mathbf{j}_s$, Eq. (22) reduces to $\mathbf{F}_{\rm int} = -\eta\dot{\mathbf{u}}-\alpha\hat{z}\times\dot{\mathbf{u}}$ as used in Eq. (21) with

$$\eta=\frac{1}{1+(\omega_e\tau)^2}\frac{\phi_0 B_{c2}L_c}{\rho_n}=\frac{\omega_e\tau}{1+(\omega_e\tau)^2}\pi\hbar n_s L_c, \tag{24}$$

$$\alpha=\eta\omega_e\tau. \tag{25}$$

Here ρ_n is the normal-state resistivity and $\tau=m_e/n_e e^2\rho_n$ the elastic scattering time of the electrons in the vortex core with m_e, n_e, and e, respectively, the mass, particle density, and charge of the electrons and $n_s=n_e$[34] the density of superconducting electrons. $\hbar\omega_e\cong\hbar^2/2m_e\xi_{ab}^2=\hbar eB_{c2}/m_e\equiv\Delta E$ is the energy separation between the lowest levels of the electrons localized in the vortex core in a free-electron approximation. According to the uncertainty principle the width δE of these energy levels can be estimated by $\delta E\cong\hbar/\tau$. Therefore the magnitude of the parameter $\omega_e\tau\cong\Delta E/\delta E$ obviously is a measure of the ''electronic dirtiness'' of the HTS under consideration, since the level width δE becomes bigger in dirtier materials with higher impurity density and smaller τ. The interpretation of $\omega_e\tau$ as ''dirtiness parameter'' is further supported by the notion that ω_e alternatively can be seen as the cyclotron frequency of the electrons in the vortex core in the virtual presence of a magnetic field as high as B_{c2}. The dissipative term $\eta\dot{\mathbf{u}}$ thus originates from the Ohmic resistivity in the core and is dominant in dirty materials with $\omega_e\tau = \alpha/\eta\ll 1$. On the contrary, the term $\alpha\hat{z}\times\dot{\mathbf{u}}$ which originates from the Hall effect, dominates in clean materials with $\omega_e\tau \geqslant 1$ and is nondissipative. In most cases the mass term $m\ddot{\mathbf{u}}$ can be neglected with respect to the dissipative and Hall terms. But in extremely dirty materials with high ρ_n and $\omega_e\tau\to 0$ only small current densities can be generated in the vortex core and the interaction of the vortex with the host material vanishes. Then the problem reduces to the well-known case of *massive* tunneling where the mass is determining the vortex dynamics.

From the equation of motion Eq. (21) $\langle u^2\rangle$ can be calculated both for quantum and thermal fluctuations using[35]

$$\langle u^2\rangle=\frac{\int Du\,\Sigma_{n=-\infty}^{\infty}u_n u_{-n}\exp(-S_E)}{\int Du\exp(-S_E)} \tag{26}$$

with S_E the Euclidean action corresponding to Eq. (21). Here we use the notation $u_n\equiv u(\omega_n)$ with $u(\tau) = \Sigma_{n=-\infty}^{\infty}u(\omega_n)\exp(-i\omega_n\tau)$, $\omega_n=n\cdot 2\pi k_B T/\hbar$ the so-called Matsubara frequencies, k_B the Boltzmann constant, and $\tau = i\cdot t$ imaginary time. Due to the Hall term the vortex motion in the x and y direction are linked and Eq. (21) leads to two coupled differential equations. From the variational calculation $\delta S_E=0$ with

$$S_E=(k_BT)^{-1}\sum_{n=-\infty}^{\infty}[m(\omega_0^2+\omega_n^2)+\eta|\omega_n|]\cdot[u_{x,n}u_{x,-n} + u_{y,n}u_{y,-n}]+2\alpha\omega_n u_{x,n}u_{y,-n} \tag{27}$$

we regain these two differential equations after analytical continuation and therefore Eq. (27) describes the Euclidean action belonging to the equation of motion under consideration. Diagonalization of Eq. (27) and substitution of the result in the functional integral of Eq. (26) gives

$$\langle u^2\rangle=2k_BT\sum_{n=-\infty}^{\infty}\frac{m(\omega_0^2+\omega_n^2)+\eta|\omega_n|}{[m(\omega_0^2+\omega_n^2)+\eta|\omega_n|]^2+\alpha^2\omega_n^2}. \tag{28}$$

The analytical continuation of Eq. (28) yields the final expression for the mean-square displacement, which is the central result of this analysis:

$$\langle u^2\rangle=-\frac{i\hbar}{2\pi}\int_{-\infty}^{\infty}d\omega\frac{m(\omega_0^2-\omega^2)-i\eta\omega}{[m(\omega_0^2-\omega^2)-i\eta\omega]^2-\alpha^2\omega^2} \times\coth\frac{\hbar\omega}{2k_BT}. \tag{29}$$

Equation (29) contains both the temperature and the material dependence of vortex creep and in principle also the magnetic-field dependence once $k(B_e)$ is known. E.g., the quantum relaxation rate $Q(T=0)$ follows when solving Eq. (29) for $T=0$. We discuss this limit in Sec. IV D with the vortex mass and Hall term explicitly incorporated. But we now focus on the temperature dependence in the crossover and thermal regime while neglecting the mass with respect to the dissipative and Hall term. The relaxation rate for the latter temperature regime follows when solving the integral in Eq. (29) for $T\gg 0$ in which case $\coth(\hbar\omega/2k_BT)\to 2k_BT/\hbar\omega$. The result is

$$\langle u^2\rangle_{T\gg 0}=\frac{k_BT}{m\omega_0^2} \tag{30}$$

which together with Eq. (20) and $U_0\approx\frac{1}{2}m\omega_0^2u_0^2$ leads to the temperature dependence

$$Q(T\gg 0)\approx\frac{c}{2}\frac{k_BT}{U_0(T)}\frac{j_c(T)}{j_s(T)} \tag{31}$$

for thermally activated flux motion. The relaxation rate for the crossover regime between thermal activation and pure quantum tunneling at $T=0$ is calculated using

$$\langle u^2\rangle_{T\to 0}=\langle u^2\rangle_{T=0}+\frac{\hbar\eta}{\pi m^2\omega_0^4}\int_0^{\infty}\omega\left(\coth\frac{\hbar\omega}{2k_BT}-1\right)d\omega. \tag{32}$$

This leads to

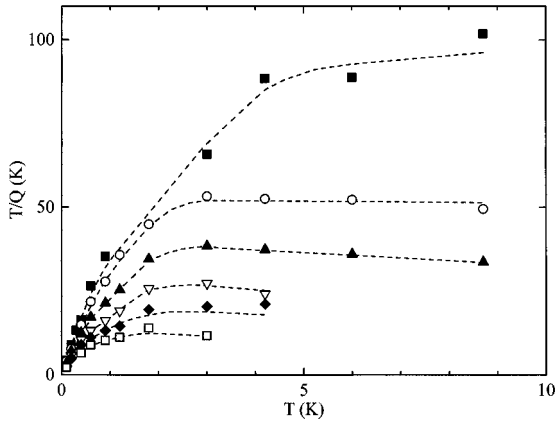

FIG. 7. T/Q vs T for the $Pr_{1.85}Ce_{0.15}CuO_{4+\delta}$ single crystal ($T_c = 23.2$ K) from which the crossover temperature T_{cr} can be determined (see text). Top to bottom: $B_e = 0.1$, 0.5, 1, 2, 3, and 5 T. Dashed lines are guides to the eye.

$$Q(T\rightarrow 0)\approx Q(T=0)+c\,\frac{2\pi\hbar}{3\hbar}\left(\frac{k_BT}{m\omega_0^2}\right)^2\frac{j_c(T)}{j_s(T)}, \qquad (33)$$

where we will evaluate $Q(T=0)$ and c further on.

B. $Q(T)$ in the crossover regime

The temperature T_{cr} which limits the crossover regime can be determined by plotting T/Q vs T (see, e.g., Fig. 7). According to Eq. (31), T/Q is constant or slowly rises with increasing T in the thermal regime, except when approaching the irreversibility temperature where Q increases much faster than T so that T/Q vanishes. However, according to Eq. (33) T/Q steeply vanishes below T_{cr} since then $T\rightarrow 0$ while $j_c(T\rightarrow 0)/j_s(T\rightarrow 0)\cong 1$ and $Q(T\rightarrow 0)$ becomes constant. The crossover temperatures determined in this way are plotted in Fig. 8 as function of B_e for the different compounds. A general feature is a roughly field independent T_{cr} at $B_e \geqslant 1$ T but the magnitude of $T_{cr}(B_e)$ is strongly sample dependent, reflecting the difference in activation energy $U(j_s,T)$. For temperatures below this T_{cr} a quadratic T dependence of Q is expected on basis of Eq. (33) and $j_c(T\rightarrow 0)/j_s(T\rightarrow 0)\cong 1$. But strikingly, linear fits to the $Q(T)$ curves in Fig. 5 (solid lines) are much better below T_{cr}. Only in case of the $Tl_2Ba_2CaCu_2O_8$ thin film for $B_e \leqslant 2$ T, the $Tl_2Ba_2Ca_2Cu_3O_{10}$ thin film which was investigated for $B_e \leqslant 0.3$ T and the $Pr_{1.85}Ce_{0.15}CuO_{4+\delta}$ single crystal with $T_c = 12.1$ K for $B_e \leqslant 1$ T a quadratic fit is favorable. Based on a semiclassical calculation a linear T dependence of Q in the crossover regime is predicted by Ao and Thouless[31] for weak pinning in clean materials. However, this prediction does not apply to the $Pr_{1.85}Ce_{0.15}CuO_{4+\delta}$ single crystals since these are in the dirty limit, i.e., $\omega_e\tau \ll 1$ (see Sec. IV D). Further, it is unlikely that the remaining linear temperature dependence of Q is caused by a residual temperature dependence of j_c or of the viscosity η (i.e., of L_c, B_{c2}, or ρ_n) in Eq. (33). Like $B_{c2}(T)=B_{c2}(0)[1-(T/T_c)^2]/[1+(T/T_c)^2]$, j_c and L_c are predicted to be effectively temperature independent for $T\rightarrow 0$ in all present theories {i.e., $j_c(T)\propto[1+(T/T_c)^2]^{5/6}[1-(T/T_c)^2]^{7/6}$ and $L_c(T)\propto[1+(T/T_c)^2]^{1/3}[1-(T/T_c)^2]^{-1/3}$ for weak collective pinning of single vortices[36]}. For $\rho_n(T)$ to cause the linear temperature behavior of Q below T_{cr} ρ_n near $T=0$ should increase linearly with increasing T for dirty HTS's, but instead we find either no T dependence or a decrease of ρ_n with increasing T, e.g., for the $Pr_{1.85}Ce_{0.15}CuO_{4+\delta}$ single crystals with $T_c = 23.2$ K and $T_c = 12.1$ K, respectively.[7] From Eq. (33) an increase of the pinning constant $k\cong m\omega_0^2$ with T in the crossover regime seems to remain as a possible cause. This T dependence of k should vanish then at lower B_e to recover the T^2 dependence as measured for $Tl_2Ba_2CaCu_2O_8$, $Tl_2Ba_2Ca_2Cu_3O_{10}$, and $Pr_{1.85}Ce_{0.15}CuO_{4+\delta}$ at low magnetic fields. We have to conclude, however, that the linear dependence observed in many samples is presently not understood.

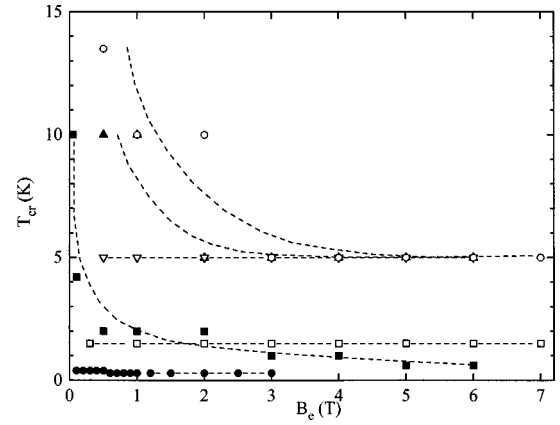

FIG. 8. T_{cr} vs B_e for the $YBa_2Cu_3O_{7-\delta}$ single crystal (□), $YBa_2Cu_3O_{7-\delta}$ thin film (○), $YBa_2Cu_4O_8$ thin film (▲), $Tl_2Ba_2CaCu_2O_8$ thin film (▽), $Pr_{1.85}Ce_{0.15}CuO_{4+\delta}$ single crystals with $T_c = 23.2$ K (■), and $T_c = 12.1$ K (●). Dashed lines are guides to the eye.

C. Field dependence of quantum creep

For comparison, Figs. 9(a)–9(f) show Q versus B_e for the various HTS's examined in this work. Crosses and solid lines show the field dependence of the extrapolated $Q(T=0)$ for every compound. From Fig. 9(a) we find that for the $YBa_2Cu_3O_{7-\delta}$ single crystal Q decreases with B_e between 0 and 7 T for $T \leqslant 3$ K, but at higher temperatures this turns into $Q\propto B_e$ above an ever lower field [inset Fig. 9(a)]. In order to explore whether or not twin planes can lead to this peculiar field dependence, we cut the originally measured $YBa_2Cu_3O_{7-\delta}$ single crystal into three pieces, one part heavily twinned, one with only two twins and the other without twins, and measured $Q(B_e)$ for the latter two parts at $4.2 \leqslant T \leqslant 20$ K. We found hardly any difference with the results in the inset of Fig. 9(a). Therefore twin planes can be ruled out as the origin of this field behavior and as cause of the difference between $Q(B_e)$ of the $YBa_2Cu_3O_{7-\delta}$ crystal and $YBa_2Cu_3O_{7-\delta}$ thin film [Fig. 9(b)]. For the latter, Q rapidly increases from nearly 0 at low fields until it saturates and slowly decreases between 1 and 7 T for $T \leqslant 3$ K. At higher temperatures the decrease turns into a linear increase with field [inset Fig. 9(b)], like for the $YBa_2Cu_3O_{7-\delta}$ single crystal. For $Bi_2Sr_2Ca_2Cu_3O_{10}$ granular material a similar transition from rapid increase to saturation of Q with B_e has been reported at low T (Ref. 37) and was attributed to a three-dimensional–two-dimensional (3D-2D) crossover of the vortex ensemble. However, a 3D-2D crossover field of

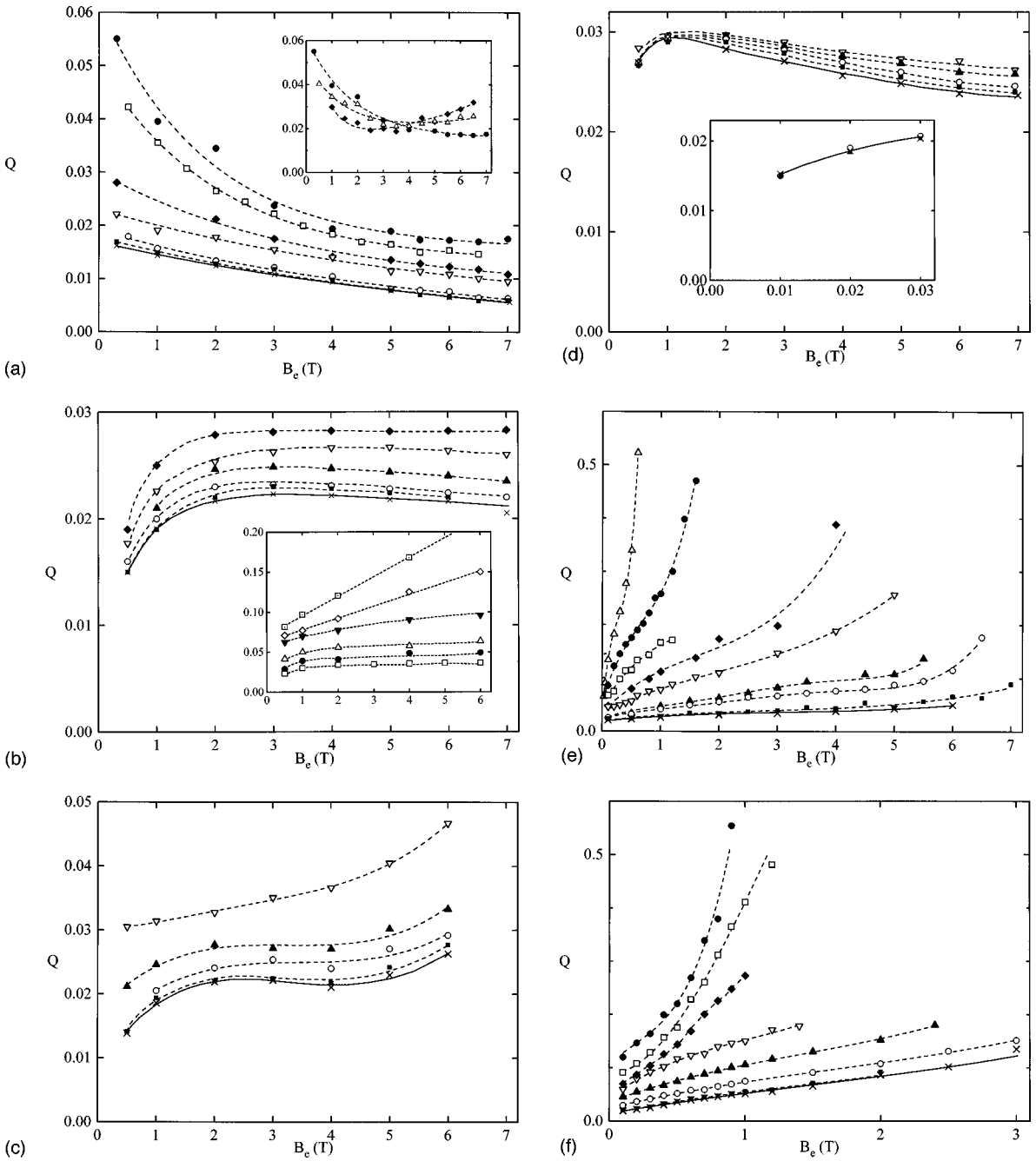

FIG. 9. (a) Q vs B_e for the $YBa_2Cu_3O_{7-\delta}$ single crystal. Crosses and solid lines are the extrapolated $Q(T=0)$, dashed lines are guides to the eye. From top to bottom: $T=4.2$, 3, 1.5, 1, 0.2, and 0.1 K. Inset: $T=4.2$ (●), 10 (△), and 15 K (◆). (b) Q vs B_e for the $YBa_2Cu_3O_{7-\delta}$ thin film. From top to bottom: $T=1.5$, 1, 0.6, 0.3, and 0.1 K. In the inset from top to bottom: $T=67$, 59.6, 41.8, 22.3, 13.6, and 4.2 K. (c) Q vs B_e for the $YBa_2Cu_4O_8$ thin film. From top to bottom: $T=4.2$, 1.6, 0.7, and 0.2 K. (d) Q vs B_e for the $Tl_2Ba_2CaCu_2O_8$ thin film. From top to bottom: $T=1.1$, 0.7, 0.3, and 0.1 K. Inset: Q vs B_e for the $Tl_2Ba_2Ca_2Cu_3O_{10}$ film. Data for $T\leqslant 1.5$ K coincide and for clarity only points for $T=1.5$ (○) and 0.1 K (■) are shown. (e) Q vs B_e for a $Pr_{1.85}Ce_{0.15}CuO_{4+\delta}$ single crystal ($T_c=23.2$ K). From top to bottom: $T=12.9$, 8.7, 6, 4.2, 3, 1.2, 0.9, and 0.1 K. (f) Q vs B_e for a $Pr_{1.85}Ce_{0.15}CuO_{4+\delta}$ single crystal ($T_c=12.1$ K). From top to bottom: $T=2.5$, 2.1, 1.7, 1.2, 0.7, 0.4, and 0.1 K.

the order of 50 T is theoretically expected for $YBa_2Cu_3O_{7-\delta}$ in contrast to the crossover at ~1 T observed in our experiments. We attribute this transition and the difference in low-field behavior between a single crystal and a thin film of the same compound at low T to the presence of strong pinning centers in thin films. These will prevent vortex motion and suppress the relaxation rate until all strong pinning sites are occupied by vortices at a certain matching field. The presence of strong pinning sites then should be common to films since we also find the suppression of Q at low fields in the $YBa_2Cu_4O_8$, $Tl_2Ba_2CaCu_2O_8$, and $Tl_2Ba_2Ca_2Cu_3O_{10}$ films [respectively, Figs. 9(c), 9(d), and inset of Fig. 9(d)] as well as in $[YBa_2Cu_3O_7]_n/[PrBa_2Cu_3O_7]_m$ multilayers[38] and $YBa_2Cu_3O_x$ thin films with various oxygen content x.[39] For the $Tl_2Ba_2Ca_2Cu_3O_{10}$ film $Q(T,B_e)$ was measured down to $B_e=0.01$ T with a torque meter especially sensitive at low

fields. For the latter data a straightforward extrapolation of $Q(B_e)$ to $B_e=0$ T is troublesome due to the demagnetization field which is of the order of 0.02 T for this sample.

Although at higher T the relaxation rates are very different in magnitude for the various compounds in Figs. 9(a)–9(d) the values of $Q(T=0)$ are remarkably similar above the matching fields [e.g., $Q(T=0,B_e=1\text{ T})\cong 0.022$]. This then seems to be a general feature of clean HTS's since these compounds all are in the clean limit, as will be shown in Sec. IV D. In Figs. 9(e) and 9(f) can be seen that for both $Pr_{1.85}Ce_{0.15}CuO_{4+\delta}$ single crystals the values of $Q(T=0)$ at fixed field are structurally higher than for the clean HTS's treated above. In the analysis performed in Sec. IV D we will show that this is related to the fact that the $Pr_{1.85}Ce_{0.15}CuO_{4+\delta}$ are dirty HTS's for which $Q(T=0)\propto 1/\eta(0)$ [see Eq. (39) below]. Based on a calculation by Volovik,[40] Parks *et al.*[41] propose that for a *d*-wave superconductor η has to be replaced by $\eta\sqrt{(B_e/B_{c2})}$ which directly would lead to $Q(T=0)\propto 1/\sqrt{B_e}$ in case of the dirty $Pr_{1.85}Ce_{0.15}CuO_{4+\delta}$. However, we find essentially $Q(T=0)\propto B_e$.

In our analysis it is assumed that the vortex system is in the single vortex regime, i.e., vortex segments tunnel individually. This assumption is reasonable since according to present theories only in this regime the tunneling rate is sizeable and tunneling of vortex bundles would lead to negligible quantum creep rates. Moreover, a strong decrease of $Q(T=0)$ with increasing B_e is expected in case of collective creep. E.g., for small bundles in highly anisotropic HTS's the quantum creep rate depends on B_e as $Q(T=0)\propto[j_c(B_e)/B_e]^4$ [Ref. 42(a)] and in less anisotropic HTS's as $Q(T=0)\propto B_e^{1/2}\exp-[B_e/j_c(B_e)]^{3/2}$.[42(b)] This is inconsistent with the field dependencies of $Q(T=0)$ observed for the various samples considered in this work. E.g., the $Pr_{1.85}Ce_{0.15}CuO_{4+\delta}$ single crystal with $T_c=23.2$ K is highly anisotropic for $T=0.1$ K and $B_e\leqslant B_\gamma=3.2$ T since then $L_c\cong(\xi_{ab}/\gamma^{4/3})[j_0/j_c(B_e)]^{1/2}$ [Ref. 42(c)] is smaller than the separation $d\approx 1.2$ nm between the superconducting CuO_2 planes. Here $\gamma\equiv\sqrt{(m_z/m)}\cong 55$ is the anisotropy,[43] $j_0(0)\equiv\phi_0/3\pi\sqrt{3}\mu_0\lambda_{ab}^2(0)\xi_{ab}(0)\approx 2.4\times10^{12}$ A/m^2 the depairing current density (see for parameter values Table I of Ref. 7), $j_c(T\to0,B_e)\approx j_s(T\to0,B_e)$ and $j_s(T=0.1\text{ K},B_e)\approx 1.6\times10^{10}\exp(-0.8B_e)$ A/m^2. In contrast to a strong decrease of $Q(T=0)$, an almost linear increase of $Q(T=0)$ with B_e is observed for this compound above as well as below $B_\gamma=3.2$ T, indicating that quantum creep can only occur in the single vortex limit. In Sec. IV D we therefore compare $Q(T=0)$ measured for the various samples with the results of single vortex tunneling theory at, e.g., $B_e=1$ T. This field is large enough to be above any matching field determined by strong pinning and low enough to avoid collective creep. Furthermore, at this field all the HTS's investigated in this work are highly anisotropic except for the $YBa_2Cu_3O_{7-\delta}$ and $YBa_2Cu_4O_8$ samples, which have only moderate γ.

D. Material dependence of $Q(T=0)$

Finally, we focus on the quantum limit and the dependence of vortex tunneling on the interaction with the host material, i.e., the variation of $Q(T=0)$ with $\omega_e\tau$. Both in the work of Caldeira and Leggett[3(a)] and Larkin and Ovchinnikov[29] the tunneling probability at $T=0$ in presence of dissipation is calculated semiclassically for a one-dimensional cubic pinning potential $U_{\text{pin}}(x)=3U_0(x/x_0)^2(1-2x/3x_0)$. Since in HTS's $U_0\gg\hbar\omega_0$ the WKB approximation is applicable and the probability of *massive* tunneling (i.e., without interaction with the environment) becomes $P_{\text{mt}}\propto\exp-36U_0/5\hbar\omega_0$.[3(c)] Using the approximation $U_0\approx 1/2m\omega_0^2x_0^2$ this leads to

$$P_{mt}\propto\exp-\frac{18}{5}\frac{m\omega_0x_0^2(1-j_s/j_c)}{\hbar} \tag{34}$$

which is reliable up to a factor of order unity in the exponent. In the aforementioned work dissipation is generally modeled by a coupling of the tunneling object to a bath of harmonic oscillators, leading to an extra term $\pi\eta x_0^2/2\hbar$ in the tunneling exponent of Eq. (34). Therefore *dissipative* tunneling dominates *massive* tunneling when $\eta>(36/5\pi)(m\omega_0)$ leading to

$$P_{dt}\propto\exp-\frac{\pi}{2}\frac{\eta x_0^2(1-j_s/j_c)}{\hbar}. \tag{35}$$

Although the prefactor of the exponential function in Eq. (34) is also affected by dissipation, we neglect it since it does not contribute to the relaxation rate Q. The parameter η is intricately connected to the dynamics of the bath of harmonic oscillators and corresponds to the phenomenological friction coefficient (or viscosity) in the damped equation of motion of the tunneling object. When the object is a vortex, dissipation occurs as discussed in Sec. IV A and η is given by Eq. (24). However, in clean HTS's the vortex tunneling is dominated by the Hall effect in the vortex core and Eq. (35) is not applicable. The Hall effect has been included by Feigel'man *et al.*[44] in a semiclassical calculation of the tunneling probability which yields

$$P_{ht}\propto\exp-\pi n_sV(1-j_s/j_c) \tag{36}$$

for the probability of Hall tunneling with $V\propto L_cu_0^2$ the volume spanned by the tunneling trajectory of the vortex. However, instead of treating these cases separately, we can also use Eqs. (19) and (29) to calculate an expression for the tunneling probability incorporating both the effects of mass and dissipation as well as of the Hall effect. The tunneling exponent would be correct except for a factor c, which can be determined by comparison with the results of the correct semiclassical calculations or with measurements. We therefore solve the integral in Eq. (29), while explicitly including the vortex mass and Hall term for $T=0$. In this case $\coth(\hbar\omega/2k_BT)\to 1$ and we find

$$\langle u^2\rangle_{T=0}=\frac{\hbar}{\pi\eta}\frac{1}{R_+^2+R_-^2}\left(\frac{R_+}{2}\ln\frac{(R_-+\alpha/\eta)^2+(1+R_+)^2}{(R_--\alpha/\eta)^2+(1-R_+)^2}+R_-\operatorname{arctg}\frac{R_--\alpha/\eta}{1-R_+}+R_-\operatorname{arctg}\frac{R_-+\alpha/\eta}{1+R_+}\right),$$

$$R_{\pm}=\frac{1}{\sqrt{2}}\sqrt{\sqrt{(1-(\alpha/\eta)^2-(2m\omega_0/\eta)^2)^2+4(\alpha/\eta)^2}\pm(1-(\alpha/\eta)^2-(2m\omega_0/\eta)^2)}. \tag{37}$$

Thus $\langle u^2\rangle$ depends explicitly on the host material, on the pinning mechanism, and on the vortex mass by way of the dirtiness parameter $\alpha/\eta=\omega_e\tau$, the prefactor $1/\pi^2 n_s L_c$, and the term $2m\omega_0/\pi\hbar n_s L_c$.

As before, the corresponding expressions for the relaxation rate Q can be derived by solving the flux creep Eq. (3) with respect to j_s after replacing $P_{\rm ta}$ by the above expressions for the tunneling probability. Using $j_c(T=0)\approx j_s(T=0)$ and $x_0\approx\xi_{ab}(0)$ [Ref. 42(e)] for dirty compounds where vortex motion is mainly perpendicular to $\mathbf{j}_s$, we then find

$$Q_{\rm mt}(T=0)\cong\frac{5}{18}\frac{\hbar}{m\omega_0\xi_{ab}^2(0)} \tag{38}$$

independent of $\omega_e\tau$ for *massive* tunneling,

$$Q_{\rm dt}(T=0)\approx\frac{2}{\pi}\frac{\hbar}{\eta(0)\xi_{ab}^2(0)} \tag{39}$$

$$\approx\frac{2}{\pi^2}\frac{1}{n_s L_c(0)\xi_{ab}^2(0)}\frac{1}{\omega_e\tau} \tag{40}$$

independent of m for *dissipative* tunneling and

$$Q_{\rm ht}(T=0)\approx\frac{1}{\pi n_s V} \tag{41}$$

independent of $\omega_e\tau$ and m for *Hall* tunneling. The interpolation formula for arbitrary $\omega_e\tau$ becomes

$$Q(T=0)\approx\frac{c\langle u^2\rangle}{u_0^2} \tag{42}$$

with $\langle u^2\rangle$ given by Eq. (37). In the limit $\omega_e\tau\ll 1$ we find

$$Q(T=0)\approx\frac{c}{2}\frac{\hbar}{m\omega_0\xi_{ab}^2(0)}\left(1-\frac{\eta}{\pi m\omega_0}\right), \tag{43}$$

implying that *dissipative* tunneling dominates *massive* tunneling when $\eta>0.1\pi m\omega_0$. This condition for *dissipative* tunneling is more accurate than the one found before. An estimation of the term $m\omega_0$ can be made by combining

$$m\omega_0^2\approx\frac{2U_0}{x_0^2}\approx\frac{2\phi_0 L_c j_c}{\xi_{ab}} \tag{44}$$

and the expression for the electromagnetic contribution to the vortex mass[45]

$$m_{\rm em}=\frac{\varepsilon_0 L_c}{4\pi}\left(\frac{\phi_0}{\xi_{ab}}\right)^2, \tag{45}$$

which outweighs the contributions of, e.g., phonon drag and electron drag by the vortex core. This leads to

$$m\omega_0\approx L_c\left(\frac{\varepsilon_0 j_c}{2\pi}\right)^{1/2}\left(\frac{\phi_0}{\xi_{ab}}\right)^{3/2} \tag{46}$$

with ε_0 the dielectrical constant. We therefore conclude that for $(0.1/\hbar n_s)(\varepsilon_0 j_c/2\pi)^{1/2}[\phi_0/\xi_{ab}(0)]^{3/2}<\omega_e\tau\ll 1$ vortex tunneling will be *dissipative* so that Eqs. (39) and (40) can be applied, while for values of $\omega_e\tau$ below this range tunneling will be *massive* so that Eq. (38) is applicable. For $\omega_e\tau\gtrsim 1$ *Hall* tunneling will dominate vortex motion at $T=0$ and the quantum creep rate then is given by Eq. (41). To decide about the regime in which tunneling occurs, one first has to estimate the value of

$$\omega_e\tau\cong\frac{\hbar}{2e^2}\frac{1}{n_e\rho_n(0)\xi_{ab}^2(0)} \tag{47}$$

for the HTS under consideration. In Tables I and II of Ref. 7 values are summarized of the relevant parameters at $B_e=1$ T for HTS's considered in this and earlier work (viz. $[YBa_2Cu_3O_7]_n/[PrBa_2Cu_3O_7]_m$ multilayers with $n=1$, 2, 3 and $m=8$,[38] $YBa_2Cu_3O_x$ thin films with $x=6.55$, 6.6, and 6.7,[39] and a $Bi_2Sr_2CaCu_2O_8$ single crystal[46]). Only for the HTS's in Table I of Ref. 7 $\rho_n(0)$ can be reliably found by linear extrapolation of $\rho_n(T)$ to $T=0$ for $T<T_c$, since T_c is low and the magnitude of $\rho_n(T_c)$ is high. For the samples in Table II of Ref. 7 only an upper limit of $\rho_n(0)$ can be estimated. Furthermore, $B_{c2}(0)$ falls within our experimental range only for the $Pr_{1.85}Ce_{0.15}CuO_{4+\delta}$ samples [with $B_{c2}(0)\approx 6$ T and ≈ 10 T for the sample with $T_c=12.1$ and 23.2 K, respectively] so that $\xi_{ab}(0)=[\phi_0/2\pi B_{c2}(0)]^{1/2}$ can be determined accurately from resistivity measurements. The Werthamer formula $B_{c2}(0)\approx -0.7 dB_{c2}/dT]_{T_c}T_c$ has to be used to evaluate $\xi_{ab}(0)$ for the other samples. From the $\omega_e\tau$ values it is clear that vortex tunneling is *dissipative* for the samples in Table I of Ref. 7, while for the samples in Table II of Ref. 7 quantum creep is controlled by *Hall* tunneling.

Equation (39) for *dissipative* tunneling, therefore, is applicable to the samples in Table I of Ref. 7. It shows explicitly that the quantum creep rate $Q(T=0)$ can be used to measure the viscosity $\eta(0)$. Since also $\omega_e\tau$ and n_s are reliably known for these compounds, we then are able to determine $L_c(0)$ by way of Eq. (24). Moreover, the samples in Table I are all strongly layered and theoretically one expects that in their case $L_c(0)$ should be replaced by d [Ref. 42(d)] (≈ 1.2 nm for these compounds). However, we find that $L_c(0)$ has to be replaced by a much larger quantity $L_{\rm eff}\approx 2.1\xi_{ab}(0)$. This can be seen in Fig. 10 where the dimensionless quantity $\eta(0)/\pi\hbar n_s L_c(0)$ is plotted versus $\omega_e\tau$ for the various HTS's in Table I with $L_c(0)$ replaced by d (small symbols), $L_c(0)$ replaced by $L_{\rm eff}\approx 2.1\xi_{ab}(0)$ (big symbols), and according to the theoretical prediction Eq. (24) (solid line). Clearly, the theoretical curve only fits the data for $L_{\rm eff}\approx 2.1\xi_{ab}(0)$. As reported before[7] we propose that $L_{\rm eff}$

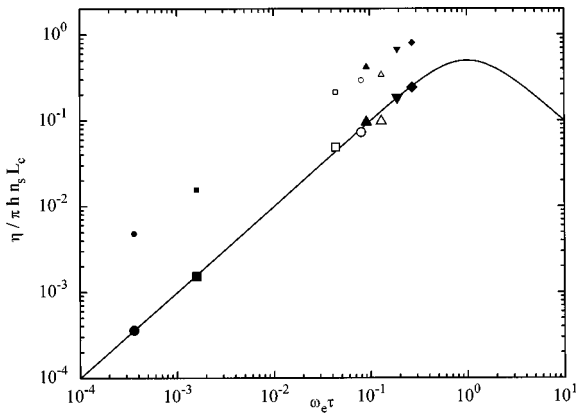

FIG. 10. The normalized viscosity versus the parameter $\omega_e\tau$ at $T=0$ K and $B_e=1$ T according to Eq. (24) (solid line) and determined for the dirty high-T_c superconductors in Table I using Eq. (39) with $L_c=d$ (small symbols) and $L_c=L_{\rm eff}\approx 2.1\xi_{ab}(0)$ (large symbols). The symbols are explained in Table II.

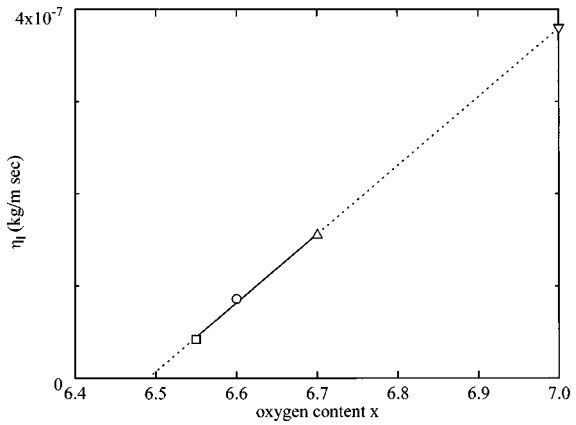

FIG. 11. The viscosity per unit length η_l at $T=0$ K versus oxygen content x for $YBa_2Cu_3O_x$ thin films. $\eta(0)$ is determined via the quantum creep rate $Q(T=0)$ [see Eq. (39)] for the dirty films with $x=6.55$, 6.6, and 6.7, while it is determined via high frequency surface impedance measurements for $x=7$.[4]

corresponds to the length of the volume in which dissipation takes place when a vortex moves, which in highly anisotropic materials could be larger than the length $L_c=d$ of the volume segment which is actually moving in highly anisotropic HTS's. This might be due to the fact that vortex motion generates not only a homogeneous electric field $\mathbf{E}=B_{c2}\hat{z}\times\dot{\mathbf{u}}$ inside the normal core but also a dipolar electric field outside the core, causing dissipation over a vertical distance of the order of ξ_{ab} in both directions. In the case of highly anisotropic dirty HTS's we therefore have to replace L_c in Eqs. (22) and (24) (and subsequent equations) by $L_{\rm eff}$. Within the class of dirty HTS's we expect the assumption $L_c=L_{\rm eff}$ of the standard Bardeen-Stephen theory to be valid only for materials with low anisotropy, where the moving vortex segments have length $L_c\gg d$.

Having determined $L_{\rm eff}$ we can calculate the viscosity $\eta_l(0)$ per unit length using Eq. (24) and the definition $\eta_l(0)=\eta(0)/L_{\rm eff}\approx 0.95\hbar/\pi Q(0)\xi_{ab}^3(0)$. The $\eta_l(0)$ values obtained in this way for the $YBa_2Cu_3O_x$ samples are plotted in Fig. 11 versus the oxygen content x. Interestingly, these values are comparable to the value for $YBa_2Cu_3O_7$ found from high-frequency surface impedance measurements (down triangle).[4] The data imply a (linear) increase of $\eta_l(0)$ with x, which is realistic since $YBa_2Cu_3O_x$ becomes less dirty for higher x.

TABLE II. Values of the parameter $\omega_e\tau$ and the multiplicative constant c in the exponent of the tunneling probability as determined for various dirty high-T_c superconductors.

	$\omega_e\tau(T=0)$	c	Symbol
$Pr_{1.85}Ce_{0.15}CuO_{4+\delta}$, $T_c=12.1$ K	0.0004	0.19	●
$Pr_{1.85}Ce_{0.15}CuO_{4+\delta}$, $T_c=23.2$ K	0.002	0.18	■
$YBa_2Cu_3O_{6.55}$ thin film	0.044	0.17	□
$YBa_2Cu_3O_{6.6}$ thin film	0.082	0.17	○
$(YBa_2Cu_3O_7)_1/(PrBa_2Cu_3O_7)_8$	0.090	0.17	▲
$YBa_2Cu_3O_{6.7}$ thin film	0.130	0.16	△
$(YBa_2Cu_3O_7)_2/(PrBa_2Cu_3O_7)_8$	0.189	0.15	▼
$(YBa_2Cu_3O_7)_3/(PrBa_2Cu_3O_7)_8$	0.268	0.15	◆

Once the value of $L_{\rm eff}$ has been recovered we also have the opportunity to experimentally determine values of the dimensionless quantity $Q(T=0)n_sL_c\xi_{ab}^2$ for the HTS's in Table I of Ref. 7 and compare them with $Q(T=0)n_sL_c\xi_{ab}^2=(2/\pi^2)(1/\omega_e\tau)$ predicted by Eq. (40) which is appropriate for *dissipative* tunneling. In the inset of Fig. 12 $Q(T=0)n_sL_c\xi_{ab}^2$ is plotted as a function of $\omega_e\tau$ and clearly the experimental data with L_c replaced by $L_{\rm eff}$ (symbols) agree well with the theoretical prediction of Eq. (40) (dotted line). For these compounds there is also the opportunity to determine the factor c in the interpolation formula Eq. (42), which predicts a value $Q(T=0)n_sL_c\xi_{ab}^2\approx c\langle u^2\rangle n_sL_c$ with $\langle u^2\rangle$ given by Eq. (37). The value of our interpolation formula should coincide with the one calculated by way of Eq. (40) (and with the experimentally determined one) at the value of $\omega_e\tau$ of the HTS under consideration. For example, for

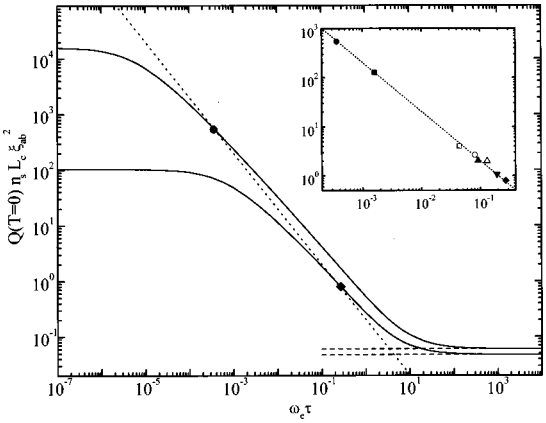

FIG. 12. The dimensionless quantity $Qn_sL_c\xi_{ab}^2$ versus the parameter $\omega_e\tau$ at $T=0$ K and $B_e=1$ T according to Eq. (40) (dotted line), determined experimentally (symbols) and according to Eq. (42) for $Pr_{1.85}Ce_{0.15}CuO_{4+\delta}$ with $T_c=12.1$ K and $[YBa_2Cu_3O_7]_3/[PrBa_2Cu_3O_7]_8$ (upper and lower solid line with $c=0.19$ and 0.15, respectively) and to Eq. (48) (dashed lines). Inset: the same quantities but now only according to Eq. (40) (dotted line) and determined experimentally for all the highly anisotropic dirty HTS's in Table II (symbols).

$Pr_{1.85}Ce_{0.15}CuO_{4+\delta}$ single crystal with $T_c = 23.2$ K the value of $Q(T=0)n_s L_c \xi_{ab}^2 \approx c\langle u^2\rangle n_s L_c$ coincides at $\omega_e\tau = 0.0016$ with $Q(T=0)n_s L_c \xi_{ab}^2 = (2/\pi^2)(1/\omega_e\tau)$ [and with the experimentally determined $Q(T=0)n_s L_c \xi_{ab}^2 \approx 127$] for $c \approx 0.18$. The values of c obtained in this way for the other dirty compounds are reported in Table I of Ref. 7. We find that c systematically decreases with increasing $\omega_e\tau$ in the investigated $\omega_e\tau$ regime. This decrease agrees with a higher value $c(\omega_e\tau \to 0) \cong \frac{10}{18} \approx 0.56$ which follows from a comparison of Eq. (43) with Eq. (38) for the *massive* limit. In Fig. 12 we plot $Q(T=0)n_s L_c \xi_{ab}^2$ as a function of $\omega_e\tau$ according to the interpolation formula for, e.g., $Pr_{1.85}Ce_{0.15}CuO_{4+\delta}$ with $T_c = 23.2$ K, $c = 0.17$ and for $[YBa_2Cu_3O_7]_3/[PrBa_2Cu_3O_7]_8$, $c = 0.15$ (upper and lower solid line, respectively). Further $Q(T=0)n_s L_c \xi_{ab}^2$ is also plotted according to Eq. (40) for *dissipative* tunneling (dotted line) and according to

$$Q(T=0) \approx \frac{c}{\pi n_s L_c(0) u_0^2} \tag{48}$$

(dashed line) to which the interpolation formula reduces for $\omega_e\tau \gg 1$, i.e., in the case of *Hall* tunneling with u_0 replaced by $\xi_{ab}(0)$. From the solid lines it is clear that in these two compounds vortex tunneling is indeed *dissipative*. *Massive* tunneling would have played a role only if $\omega_e\tau$ would have been smaller than 6×10^{-7} (7×10^{-5}), while *Hall* tunneling would have dominated for $\omega_e\tau \geqslant 1$. Thus, unlike the crossover value between *massive* and *dissipative* tunneling the crossover value between *dissipative* and *Hall* tunneling hardly depends on the material parameters. Therefore a HTS will be in the clean limit for $\omega_e\tau \geqslant 1$ in general.

V. CONCLUSION

This paper reports on a detailed study of quantum creep in a set of representative HTS's. Below $B_e \approx 0.5$ T we observe a temperature dependence $Q(T) \propto T^2$ which is theoretically expected in the crossover regime between thermally activated and quantum motion. However, for higher fields the dependence unexpectedly turns into $Q(T) \propto T$. Such behavior is predicted by Ao and Thouless for clean materials,[31] but their theory cannot explain $Q(T) \propto T$ in $Pr_{1.85}Ce_{0.15}CuO_{4+\delta}$ since these samples are evidently in the dirty limit. An increase of $Q(T=0)$ from nearly 0 at $B_e = 0$ T to $Q(T=0) \approx 0.02$ around $B_e = 1$ T is a general feature of clean HTS *films*. We attribute this field dependence to the presence of strong pinning centers, which prevent vortex motion as long as the vortex density does not exceed that of the strong pinning sites. Finally, we propose a semiempirical interpolation formula for $Q(T=0)$ as function of the material parameter $\omega_e\tau$, which takes into account the vortex mass, dissipation and Hall effect in the vortex core. The characteristic values of $\omega_e\tau$ which separate the *massive*, *dissipative* and *Hall* tunneling regime are identified, which allows us to classify the investigated HTS's. For *highly anisotropic* dirty HTS's we find that dissipation during vortex motion takes place in a volume larger than the volume which is expected to move. We therefore propose that the Bardeen-Stephen assumption that dissipation is limited to the moving vortex segment is applicable only for the *less anisotropic* HTS's.

ACKNOWLEDGMENT

This work is part of the research program of the Dutch Stichting voor Fundamenteel Onderzoek der Materie (FOM) which is financially supported by NWO.

[1] A. C. Mota *et al.*, Phys. Rev. B **36**, 4011 (1987); , Phys. Scr. **37**, 823 (1988); J. Lensink *et al.*, Physica C **162-164**, 663 (1989); L. Fruchter *et al.*, Phys. Rev. B **43**, 8709 (1991).

[2] M. Stone, Phys. Lett. **67B**, 186 (1977); S. Coleman, Phys. Rev. D **15**, 2929 (1977); C. G. Callan and S. Coleman, *ibid.* **16**, 1762 (1977); J. P. Sethna, Phys. Rev. B **25**, 5050 (1982); A. O. Caldeira and A. J. Leggett, Phys. Rev. Lett. **46**, 211 (1981).

[3] (a) O. Caldeira and A. J. Leggett, Ann. Phys. (N.Y.) **149**, 374 (1983); (b) **149**, 378 (1983); (c) **149**, 386 (1983); (d) **149**, Appendix B (1983).

[4] M. Golosovsky, M. Tsindlekht, and D. Davidov, Supercond. Sci. Technol. **9**, 1 (1996).

[5] Other systems known to exhibit macroscopic quantum tunneling are, e.g., the flux trapped in a rf superconducting quantum interference device or the carbon-monoxide ligand bound by a myoglobin protein.

[6] M. Qvarford *et al.*, Rev. Sci. Instrum. **63**, 5726 (1992).

[7] A. F. Th. Hoekstra *et al.*, Phys. Rev. Lett. **80**, 4293 (1998).

[8] See for details of the sample preparation and characterization respectively, B. Dam *et al.*, in *High-T_c Superconducting Thin Films, Devices, and Applications* (American Institute of Physics, New York, 1989); U. Welp *et al.*, Phys. Rev. Lett. **62**, 1908 (1989); P. Berghuis *et al.*, Physica C **167**, 348 (1990); S. L. Yan *et al.*, Appl. Phys. Lett. **63**, 1845 (1993); A. García *et al.*, Phys. Rev. B **50**, 9439 (1994); M. Brinkmann *et al.*, J. Cryst. Growth **163**, 369 (1996).

[9] R. Griessen, A. Hoekstra, and R. J. Wijngaarden, Phys. Rev. Lett. **72**, 790 (1994).

[10] A. Gerber and J. J. M. Franse, Phys. Rev. Lett. **71**, 1895 (1993).

[11] A. P. Malozemoff, Physica C **185-189**, 264 (1991).

[12] H. H. Wen *et al.*, Phys. Rev. Lett. **79**, 1559 (1997).

[13] H. Schnack *et al.*, Phys. Rev. B **48**, 13 178 (1993); H. H. Wen *et al.*, Physica C **241**, 353 (1995).

[14] O. V. Lounasmaa, *Experimental Principles and Methods Below 1 K* (Academic Press, London, 1974).

[15] R. C. Weast, *CRC Handbook of Chemistry and Physics* (CRC Press, Boca Raton, FL, 1978).

[16] M. P. A. Fisher, Phys. Rev. Lett. **62**, 1415 (1989); D. S. Fisher, M. P. A. Fisher, and D. A. Huse, Phys. Rev. B **43**, 130 (1991).

[17] A. J. J. van Dalen *et al.*, Physica C **259**, 157 (1996).

[18] A. F. Th. Hoekstra, J. C. Martinez, and R. Griessen, Physica C **235-240**, 2955 (1994).

[19] G. T. Seidler *et al.*, Phys. Rev. Lett. **74**, 1442 (1995).

[20] G. Sparn *et al.*, Physica C **162-164**, 508 (1989).

[21] C. Uher, S. D. Peacor, and J. Shewcum, Physica C **177**, 23 (1991).

[22] M. Núñez Regueiro *et al.*, Phys. Rev. B **44**, 9727 (1991).

[23] B. M. Andersson and B. Sundqvist, Phys. Rev. B **48**, 3575 (1993).

[24] Cao Shao-Chun *et al.*, Phys. Rev. B **44**, 12 571 (1991).
[25] H. Ogasawara *et al.*, Physica C **235-240**, 1399 (1994).
[26] M. Jirsa *et al.*, Physica C **207**, 85 (1993).
[27] M. J. Stephen, Phys. Rev. Lett. **72**, 1534 (1994).
[28] For the quadratic potential this simply follows from $P \propto \exp -(2/\hbar)\int_0^{x_0}\sqrt{2mU(x)}dx$ and $\langle x^2\rangle = \hbar/2m\omega_0$ valid for the ground state of a harmonic oscillator with $U_0 = m\omega_0^2 x_0^2/2$.
[29] A. I. Larkin and Yu. N. Ovchinnikov, JETP Lett. **37**, 382 (1983).
[30] G. Blatter, V. B. Geshkenbein, and V. M. Vinokur, Phys. Rev. Lett. **66**, 3297 (1991).
[31] P. Ao and D. J. Thouless, Phys. Rev. Lett. **72**, 132 (1994).
[32] A derivation based on microscopic arguments is given by N. B. Kopnin and M. M. Salomaa, Phys. Rev. B **44**, 9667 (1991).
[33] J. Bardeen and M. J. Stephen, Phys. Rev. **140**, A1197 (1965).
[34] A. T. Fiory *et al.*, Phys. Rev. Lett. **65**, 3441 (1990).
[35] R. P. Feynman and A. R. Hibbs, *Quantum Mechanics and Path Integrals* (McGraw-Hill, New York, 1965), p. 325.
[36] R. Griessen *et al.*, Phys. Rev. Lett. **72**, 1910 (1994).
[37] S. Moehlecke and Y. Kopelevich, Physica C **222**, 149 (1994).
[38] A. J. J. van Dalen *et al.*, J. Alloys Compd. **195**, 447 (1993).
[39] A. J. J. van Dalen *et al.*, Phys. Rev. B **54**, 1366 (1996).
[40] G. E. Volovik, JETP Lett. **65**, 217 (1997).
[41] B. Parks *et al.*, Phys. Rev. Lett. **74**, 3265 (1995).
[42] (a) G. Blatter *et al.*, Rev. Mod. Phys. **66**, 1318 (1994); (b) **66**, 1223 (1994); (c) **66**, 2164 (1994); (d) **66**, 1214 (1994).
[43] Value obtained from torque rotation measurements around T_c for the $Pr_{1.85}Ce_{0.15}CuO_{4+\delta}$ ($T_c = 23.2$ K); to be reported.
[44] M. V. Feigel'mann *et al.*, JETP Lett. **57**, 711 (1993).
[45] H. Suhl, Phys. Rev. Lett. **7**, 226 (1965).
[46] A. J. J. van Dalen *et al.*, Physica C **257**, 271 (1996).